November 2021

# GROWTH, CHARACTERIZATION, AND MECHANICAL TESTING OF DIAMOND-LIKE CARBON FILMS

Tailei Qi

# GROWTH, CHARACTERIZATION AND MECHANICAL TESTING OF DIAMOND-LIKE CARBON FILMS

A Thesis

Submitted to the Graduate Faculty of the

Louisiana State University and

Agricultural and Mechanical College

in partial fulfillment of the

requirement for the degree of

Master of Science in Mechanical Engineering

in

The Department of Mechanical and Industrial Engineering

by

Tailei Qi

B.S., Wuhan University, 2015

December 2021

To my mother

## Acknowledgements

This thesis is completed under the guidance of Dr. Wen Jin Meng, whose effort should be sincerely appreciated. My thanks go to Dr. Shengmin Guo and Dr. Ying Wang for serving on my advisory committee.

Dr. Dongmei Cao and Dr. Yang Mu helped on the analytical facilities; Nicholas Dinecola helped me machine the parts for the plasma generating system. Dr. Ali Haghshenas helped me take the corrosion test. My work could not be done without them. The other members of Dr. Meng's research group, Dr. Bin Zhang and Dr. Xiaoman Zhang, had been my valuable partners.

Partial project support from NSF though awards OIA-1541079 and OIA-1946231 and from the Louisiana Board of Regents is gratefully acknowledged.

## Table of Contents

# List of Tables

# List of Figures

# Abstract

The high residual stresses within diamond-like carbon (DLC) films limit its thickness and make the film tend to delaminate from the substrate and be defective on the surface. To address this problem, a new plasma enhanced chemical vapor deposition system (PECVD) was set up to investigate the effects of different film growth parameters on the DLC films, such as chromium doping, gas fluxes, depositing pressures, bias voltages, and depositing times. After the film growth parameters were optimized, this condition was transferred from silicon wafer to SS316 steel plate to deposition of DLC films with some adjustments. Scanning electron microscopy (SEM) images were taken to check the surface of these DLC films. Cross-sectional SEM images were taken by cutting the DLC films with focused ion beam (FIB). Young's modulus and hardness of the DLC film were measured by instrumented nanoindentation. Multilayer DLC films with three Cr/Cr-DLC bilayers were deposited. Pure Cr interlayers were introduced to DLC films to improve its fracture toughness. Bending test of V-notched microbeams was performed on a film with a single layer of DLC and a DLC film with three Cr/Cr-DLC bilayers. The results show that by introducing more Cr interlayers in a DLC film, its fracture toughness was improved several times higher than that of a single layer DLC film.

# Chapter 1. Introduction

## 1.1. Background and properties of diamond-like carbon film

Diamond-like carbon (DLC) film was first found by Schmellenmeier when he tried to investigate the influence of acetylene gas on surfaces of tungsten-cobalt alloys [1, 2]. This carbon film didn't attract much attention until 1980s. Starting from 1990s, more and more researchers are attracted to this area and lots of papers were published [2, 3]. DLC films are distinguished by a combination favorable physical properties, high hardness, high wear resistance, low friction coefficient, high chemical stability, high insulation, and good biocompatibility[9]. These performance characteristics of DLC films offer promises in a wide range of applications, including cutting tools, gears, micro-electro-mechanical-system (MEMS) devices, protective coatings, and artificial organs [1, 3–8].

DLC films can be classified into the following groups according to its hydrogen and metal content [8]:

- α-C: hydrogen-free
- tα-C: hydrogen-free with high fraction of tetrahedral coordinated, $sp^3$ bonded carbon atoms
- α-C:Me: hydrogen-free, with incorporation of metal element(s)
- α-C:H: hydrogenated
- tα-C:H: hydrogenated, with a high fraction of tetrahedral coordinated, $sp^3$ bonded carbon atoms
- α-CH:Me: hydrogenated, with incorporation of metal element(s)
- α-CH:X: hydrogenated, with incorporation of non-metal element(s)

Thick DLC films often contain high intrinsic compressive stresses, which can cause the delamination of the film from the substrate. Incorporating metal elements (α-CH:Me) is a good way to keep most of the excellent properties while decreasing the intrinsic stress inside the film. Up to now, many metal element like Ti, Al, Mo, Co, Fe, Cr, Ni, Cu, Ca, W, Zr, Ag, Au, or non-metal elements like Si, F, B, P, have been incorporated into DLC films [6, 9–15]. For example, the presence of element F, W, and Si in DLC films can lower the coefficients of friction of the film [16–18]. Cu-doped DLC films were reported to increase surface roughness as spherical clusters of nanocrystalline particles, also Cu will deteriorate the mechanical properties of the DLC film by decreasing its hardness and Young's modulus [24]. Ag was introduced into DLC films for its antibacterial properties [25]. High biocompatibility of DLC films are expected by doping non-metal elements, e.g., N or B, or in combination with metal dopants [26].

The bonding characteristics, e.g., $sp^2/sp^3$ ratio, is another factor that determines the properties of the DLC film. DLC films contain different $sp^3$ bonded structures, which is made up of small microcrystalline or polycrystalline diamond clusters and other amorphous phases [27]. Generally, the properties of DLC films are between that of diamond and graphite. If a DLC film contains more $sp^3$ bonding, the mechanical properties of this DLC film will be closer to those of diamond. If a DLC film contains more $sp^2$ bonding, the properties of this DLC film will be closer to those of graphite. The ratio of $sp^3$ to $sp^2$ plays an important role to determine the mechanical and

electrical properties of the DLC film. It was also found that the density of DLC film increase with the $sp^3$ content until $sp^3$ content reaches a considerable value [2,3].

### 1.2. Different method to deposit diamond-like carbon film

Several methods can be used to produce DLC films.

(i) Ion beam deposition

This method uses energetic ions (e.g., methane ions, $CH_3^+$) to bombard the growth surface. The source materials, usually in the form of gases, are ionized by electron ionization, field ionization, or cathodic arc. Then these ions are accelerated by high voltages and guided by magnetic fields. Finally, these ions will bombard the surface of substrate and leave a film on the substrate. After impact, molecular ions are dissociated and hydrogen is released. During this process, ion energy between 100 eV to 700 eV can be used. Current density of about 2.5mA/$cm^2$ with an arrival rate of about $1.5*10^{16}$ atoms/$cm^2$/s can be obtained, which corresponds to a growth rate of ~0.1 μm/h [29]. DLC films obtained by this method can be very smooth and of high purity, high hardness, and high resistivity. This is quite a clean way to grow DLC films [30]. But its depositing rate is low [27].

(ii) Cathodic arc evaporation

Very hard and hydrogen-free DLC films can be grown by cathodic arc evaporation. In this method, an arc is produced between a graphite cathode and an anode. To avoid film contamination with coarse particles which are left unionized during the arc discharge, a magnetic field filter may be added to the system, as a so called filtered arc PVD method [13]. Stress in the DLC film can be -7 GPa to -10 GPa with a coating hardness up to 50 GPa [31].

(iii) Pulsed laser beam

The process of pulsed laser deposition (PLD) is simple: a pulsed laser beam hits a carbon target and causes evaporation and ablation. Then the evaporated/ablated material will be deposited into films on the substrate. There are some disadvantages of the PLD method, such as the uneven distribution and different optical penetration depths of laser beam. Plumes might be contained in the film. High-purity graphite targets are mostly used in PLD to deposit DLC films. Hardness of DLC film grown by PLD method can be 70-100 GPa [32].

(iv) Plasma enhanced chemical vapor deposition

Plasma enhanced chemical vapor deposition (PECVD) allows deposition to occur at lower temperatures. Methane ($CH_4$) or acetylene ($C_2H_2$) are introduced as a source of carbon into the space between the substrate holder and an RF-energized electrode. Ar is a common working gas to produce a plasma. Sometimes, He or other inert gases can be added to improve the plasma chemistry. A negative bias will be applied to the substrate holder [33]. Application of electric fields or combined electric and magnetic fields activates the Ar gas to produce a plasma inside the chamber. Then the ionized Ar ions will break down the precursor gases to produce carbon-containing species. PECVD is able to produce DLC films over large areas at low costs in industrial

applications. DLC films fabricated by PECVD methods typically belong to α-C:H or α-CH:Me categories when metal atoms are introduced by hybrid deposition. In this study, we used the latter method to prepare the DLC films.

### 1.3. Application of diamond-like carbon film

(i) Protective coating

DLC film is very suitable to be a protective film, due to its high hardness and chemical stability. Deposition of DLC films onto many metal objects like nails, large sheets, drills, tools, etc. have been tried to expand their durability. Because DLC films are hydrophobic, it is also used in the automobile engines such as cam-shaft bearings, plungers, and diesel injectors [34]. Now the most important application of DLC films is on the magnetic storage disks and their read heads.

(ii) MEMS

The present MEMS industry is built on fabrication technologies of silicon and/or polysilicon. However, surface of Si is hydrophilic which raises a problem of separating the devices after fabrication. In addition, Si has many other disadvantages, such as relatively large coefficients of friction, high rates of wear, and small energy band gap [35]. DLC films have hydrophobic surfaces and better mechanical and electrical properties [36]. MEMS devices built with DLC has been proven feasible [32–34]. The excellent tribological properties of DLC films, together with their chemical stability and biocompatibility offer DLC promise in applications involving biosensors, microfluidic devices, high frequency resonators, microcage, etc. [35].

(ii) Cutting tool

Low coefficients of friction and high hardness values make DLC films a highly viable coating used at the edges of razor blades. DLC coatings have a high modulus and is less ductile and will keep the blade sharp during usage. Also, DLC films are used in coating drills and micro end mills. DLC coatings are reported to enable tools to last 10-100 times longer than conventional carbide tools in similar usage [40].

(iii) Medical application

In medical applications, biocompatibility, osteointegration, hemocompatibility, or antimicrobial activity of DLC films are the most important aspects to be considered [10]. DLC has been proven to be biocompatible in both in-vitro and in-vivo studies [36, 37]. DLC has a wide potential applicability in medical situations, such as endoprosthesis and dental implants [26]. Doping of different elements allows DLC films to realize different functions. However, the amorphous nature of DLC films has a possibility to introduce detrimental elements inside DLC films, and can release into the human body at a later time and results in a short-term toxic surface [43]. Another problem that DLC films face before getting into application is pitting corrosion that might occur in-vivo after several years. If there is a pinhole in the DLC film, the corrosion process will undermine the material underneath the DLC film, until delamination of DLC film finally occurs [39, 40].

Along with the applications cited above, DLC shows desirable infrared properties. It is used in anti-reflection coatings on germanium, zinc sulfide windows, aluminum mirrors, and in solar energy conversion [46].

### 1.4. Research motivation and objective

DLC films have shown promises in a range of applications for its distinguished mechanical properties, chemical properties, electric properties, and biocompatibility. PECVD is a suitable film-deposition method to grow large area of DLC films, both in the lab and in industrial settings.

However, it has a disadvantage that high intrinsic stresses can prevent the growth of thicker films due to the tendency of film spallation. Metal element doping is a proven method that can decrease the intrinsic stress inside DLC films. However, it is still not clear by what mechanism the doped metal elements affect the DLC film. The microscopic mechanisms behind DLC-metal interactions and how they affect film properties still await further understanding.

In this study, we have built up a new PECVD system, optimized its parameters to prepare DLC films of good quality, and tested its mechanical properties using micro-mechanical testing protocols, and looked for ways to improve properties of DLC films deposited on steel substrates.

## Chapter 2. Design and construction of an inductively coupled plasmas assisted hybrid physical/chemical vapor deposition system

To obtain a thin film, many vapor phase deposition methods can be chosen. Methods like molecular-beam epitaxy (MBE), atomic layer deposition (ALD), magnetron sputtering, etc., have all been widely used for film growth. Among these, evaporated coatings are suitable for large area film production and can have cost savings in industrial applications. According to the states of matter before and after deposition, we can divide the deposition methods into physical vapor deposition (PVD) and chemical vapor deposition (CVD).

In this study, we designed and built a new plasma enhanced chemical vaper deposition (PECVD) system to deposit DLC films by using the gas of acetylene ($C_2H_2$) as the carbon feedstock.

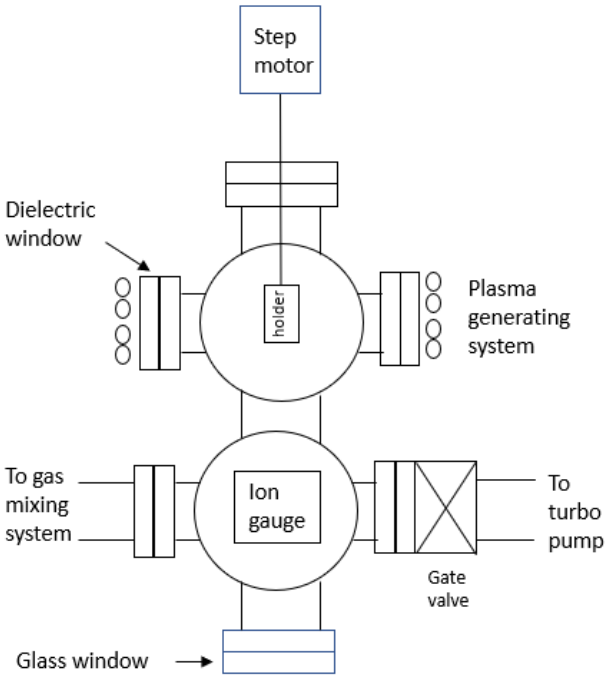


Fig 2.1. A diagrammatic sketch of the PECVD system

This PECVD system can be divided into four parts according to their functions in the depositing process:

a) vacuum pumping system;
b) plasma generating system;
c) gas handling system;
d) metal element doping system.

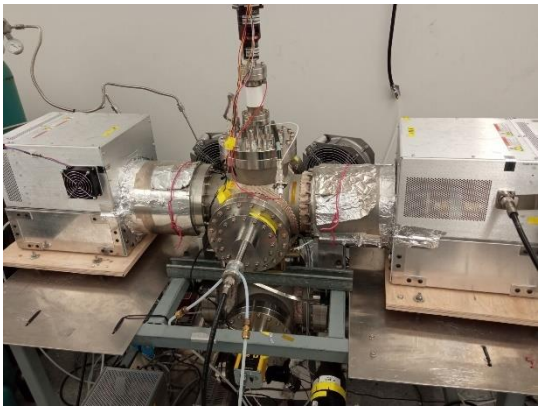

Fig 2.2. A photograph of the PECVD system.

## 2.1. Vacuum pumping system

The vacuum system is a very important part to remove contaminants inside the chamber before depositing DLC films. Usually, the base pressure of the chamber will reach to the order of $10^{-8}$ Torr before depositing DLC films to make sure most of the impurity gases have been removed.

A turbomolecular vacuum pump is used to pump down the chamber vacuum while a mechanical rotary vane pump is connected behind the turbo pump as its backing pump. No shunt tube connects the mechanical vacuum pump to the chamber directly as the total capacity of the chamber is small. A gate valve is installed between the turbo pump and the chamber. The gate valve can be used to control the pressure of the chamber by varying the effective pumping speed. When pumping down the vacuum of the chamber, the chamber is baked by two heating tapes to accelerate the pumping process.

A capacitance manometer (Baratron, MKS) was installed to gauge the pressure when gases are fed into the system. When the pressure of the chamber reaches to the order of $10^{-4}$ Torr or below, a hot cathode ionization vacuum gauge is turned on to gauge the chamber at lower pressures.

## 2.2. Plasma generating system

This part contains two radio frequency (rf) power supplies, two tuners, and two copper coils. The power supply will produce alternating electric current (13.56 MHz) in the copper coil.

The tuner will tune the total impedance of the entire circuit to be 50 Ω by an adjustable series resistance and an adjustable shunt capacitor.

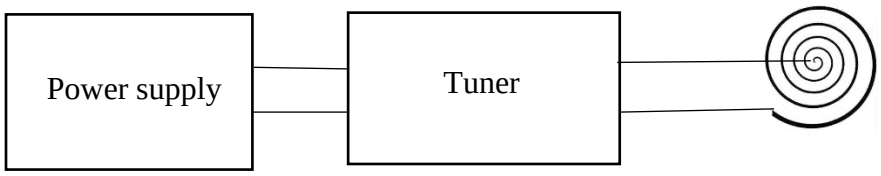


Fig 2.3. A diagrammatic sketch of the plasma generating system

Two spiral coils made with copper tubes are placed facing each other in parallel, between which is the vacuum chamber (an 8-inch six-way cross). The two spiral coils face two glass windows on the chamber. When the power supply generates an alternating electric current in the copper coil, it will in turn generate an axial magnetic field which propagates into the chamber through the glass. The axial alternating magnetic field within the chamber couples to electrons through electromagnetic induction (thus "inductive coupling"), and the energized electrons in turn ionize the argon gas into an inductively coupled plasma (ICP). Finally, the ICP will break down the $C_2H_2$ molecules thus providing the source of carbon for film deposition. An alumina plate is placed behind the glass window inside the chamber to prevent the glass window from overheating by the plasma and fracture. The copper coil and the RF power supply are cooled by flowing water during the process of DLC deposition.

A bias voltage is applied to the substrate holder with a DC power supply, typically a voltage in the range of 50 - 100V is used for the substrate bias. The bias current can be monitored by the power supply at the same time, giving an indication of the plasma density surrounding the substrate.

### 2.3. Gas handling system

Acetylene gas and argon gas are used in this PECVD system. Acetylene gas and argon gas are first flown into a mass flow meter, with a four-channel controller to control their flow rate. Then the two gases mix at a T adapter. After mixing, the mixed gas is divided again into two tubes, and injected into the chamber from the bottom and top to make the gas distribution more uniform inside the chamber. An RGA100 residual gas analyzer is also installed on the chamber to monitor the background gas content.

### 2.4. Metal element doping system

(i) Holder

An aluminum holder is used to hold the substrate for DLC film deposition. Screw is used to fix the substrate to the holder. The holder is connected to a stepping motor, which controls the holder to spin at a rate of 10 rpm. The holder is mechanically polished and cleaned to remove the DLC film after each deposition.

(ii) Magnetron sputtering

Two pure Cr targets are mounted in the chamber in the direction perpendicular to the copper coils. A magnetron sputtering gun is connect to each of the Cr targets. When depositing the DLC film, Cr atoms come off the target through sputtering and deposit on the growth surface of the substrate. It should be noted that the plasma process will also affect this process when the Cr atoms arrive in the plasma-affected zone. Metal element doping is realized when the DLC deposition by PECVD and this Cr deposition by magnetron sputtering are turned on at the same time. A metallic Cr interlayer can be obtained by only turning on the Cr magnetron sputtering process without input of $C_2H_2$ into the chamber.

# Chapter 3. Deposition of Cr doped diamond-like carbon film

## 3.1. Introduction to film growth

In a film growth process, atoms in materials will turn into vapor phase by thermal or sputtering methods. Then these atoms will be transported in the vapor phase into the area of a substrate through an inert gas filled space, usually argon. A film will be deposited on the substrate after those atoms condense into solid from vapor and accumulate at the surface of the substrate. Principles of thermodynamics is a useful tool to figure out what process those atoms have experienced in the process to grow into a film. Atoms arrive to the surface with an energy provided by the process of vaporization and released these energies when adhering to the surface. Different levels of arriving energy, interface energy, and surface energy will lead to different modes of film growth. When these atoms grow into an amorphous film, atoms are prevented from arriving at their equilibrium positions at the time they arrive at the surface.

When atoms arrive at the substrate surface, they will form chemical bonds with atoms in the substrate and become adatoms finally. In this process, energy of these atoms will decrease. Some of these atoms might gain enough energy to escape from the surface again because of thermal fluctuations. However, if the greater number of atoms are adhered to the substrate than that of escaped atoms, a film will be deposited on the substrate.

Specifically, to get a net deposition on the substrate, it is essential that the equilibrium vapor pressure $P_e$ is exceeded. That means, it is necessary for the vapor in contact to the surface to be supersaturated with respect to the substrate at that depositing temperature. And the depositing temperature should be low enough to allow the vapor phase to be supersaturated. Under the pressure P, the entropic free energy per atom above the free energy at $P_e$ can be estimated by the work needed per atoms to increase the vapor pressure from $P_e$ to P under constant temperature. By the ideal gas law, we have:

$$W = kT_v \ln \frac{P}{P_e} \tag{3.1}$$

where k is the Boltzmann constant ($1.38 \times 10^{-23} J/K$), $T_v$ is the temperature of the vapor. If the vapor becomes supersaturated, this free energy difference will drive more atoms from the vapor to adhere to the substrate and hence result in film growth. However, it should be noted that the equilibrium vapor pressure is hard to determine as the temperature of the surface is not the same with the substrate during film depositing process in practice. However, there is a limiting pressure below which the film depositing process will not occur at all. We can use this limiting pressure as the equilibrium pressure $P_e$. Similarly, if there is a step already at the surface, the free energy difference the step position and vacancy position will determine the atom whether to adhere to step to grow to a layer or adhere to the place upside the step to grow into island.

3.1.1. Modes of film growth

Once an atom has attached to the surface of substrate, it is supposed to oscillate in an equilibrium energy well with a barrier of height $\varepsilon_d$. If an atom still has enough energy higher than this energy $\varepsilon_d$, the atom will be able to jump to other adjacent positions. Such jumps will result in surface diffusion. Temperature of the substrate obviously plays an important role in this surface diffusion process. If the surface of the substrate is not uniform, surface diffusion can result in a net mass transport on a macroscopic scale. What is more, if the temperature of the substrate is not high enough, adatoms will stick to the position once they arrive and the film is likely to grow into amorphous or very fine-grained polycrystalline structure.

The modes of the film growth are determined by various energy involved in this process and their relative values. Different modes of film growth will lead to different final structure in the film. The barrier $\varepsilon_d$ energy is one of the main factors to affect the film to choose which modes it uses in the film growth process. If the barrier $\varepsilon_d$ is high compared to the background thermal energy, the adatoms will stick to the position where they arrive initially. If the barrier $\varepsilon_d$ is low compared to the background thermal energy, the adatoms will be able to move around along within the surface and find its equilibrium position finally. A high enough temperature of the substrate is very important in the growth of crystalline films to insure the mobility of adatoms.

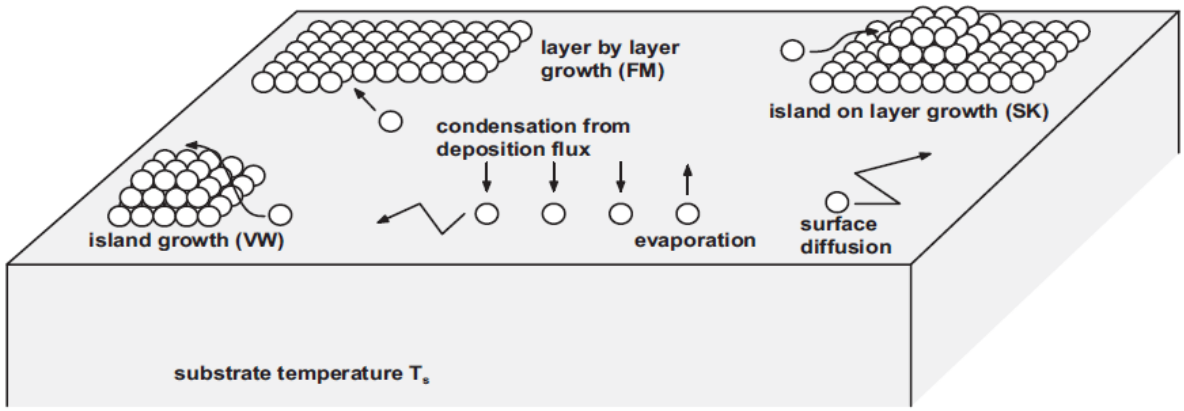


Figure 3.1. Schematic of different modes of film growth [1]

Provided that the adatoms have enough energy to move around within the surface, another parameter we should consider is to compare the tendency of the adatoms bonding to the substrate, noted as $\varepsilon_{fs}$, with the tendency of the adatoms bonding to other atoms in the film material, noted as $\varepsilon_f$. As shown in figure 3.1, three types of film growth have been recognized:

i) If $\varepsilon_{fs}$ is greater than $\varepsilon_f$, the adatoms tend to attach to the substrate first than other material surface. Then the film growth will be in a layer-by-layer mode, or often named as the *Frank-van der* Merwe growth mode or FM mode.

ii) If $\varepsilon_f$ is greater than $\varepsilon_{fs}$, the adatoms tend to attach to other atoms to form three-dimensional clusters or islands on the surface of the substrate. Then the film growth will be in an island-by-island mode, or often named as the Volmer-Weber growth mode or VW mode.

iii) The third type of the film growth mode is a combination of the two film growth modes above, or named as the *Stranski-Krastanov* growth mode. In this mode, $\varepsilon_{fs}$ is greater than $\varepsilon_f$ in the first period of film growth and the film grows in a layer-by-layer mode instead of formation clusters on the growth surface. However, after several layers of film material are formed, the relative magnitude of $\varepsilon_{fs}$ and $\varepsilon_f$ changes its sign. In other words, the atoms will turn to be more likely to attach to other atoms of film materials first after the film has been established. $\varepsilon_{fs}$ decreases during the film growth, which might be a result of the heavily strain of the film by the constraint of the substrate in the first few layers and by the different atomic properties of the substrate and the film material.

### 3.1.2. Evolution of residual stresses

It is reported that the growth mode of DLC films follows the island growth mode on silicon substrate[59]. DLC films have unusually high residual stresses inside it, which might cause the DLC film to crack or delaminate from the substrate. Research on how to decrease the residual stress has attract much attention.

Residual stress can be originated from the extrinsic stresses (mainly as thermal stresses) and intrinsic stresses. When the thermal expansion coefficients of the substrate and the film material are different, thermal stress may raise because of the temperature change. Intrinsic stresses, or so-called as growth stress, are generated during the process of film growth. Doerner and Nix have reviewed the common mechanisms for stress generation[47]. These mechanisms include:

- Surface and/or interface stress
- grain growth, or gran boundary area reduction
- vacancy annihilation
- cluster coalescence to reduce surface area
- grain boundary relaxation
- shrinkage of grain boundary voids
- incorporation of impurities
- phase transformations and precipitation
- moisture adsorption or desorption
- epitaxy
- structural damage as a result of deposition process

Most films grown on a substrate will follow the Volmer-Weber mode during the process of film growth and lead to a polycrystalline microstructure. There is a sequence of stages following the initial nucleation of island such as island growth, island coalescence, establishment of large area contiguity and filling the gaps to form a continuous film. What the role of stress plays in these stages is still not fully understood. However, some descriptive discussion can be made now.

As shown in figure 3.2, the volume-average stress is generated as compressive, then becomes as tensile, and finally stabilizes as compressive again.

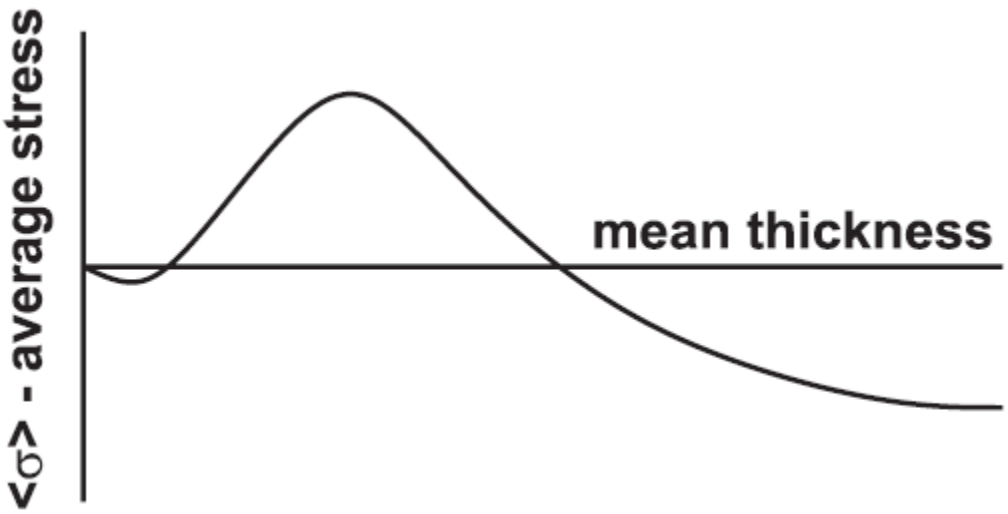


Figure 3.2. Schematic diagram of volume-average film stress versus mean film thickness during vapor deposition[1]

The initial stress is thought to because of the effect of surface and/or interface stress. The lattice spacing in a small and isolated crystallite is smaller than the spacing in a bulk crystal though they are of the same material under the same temperature. Hence, deviation of atoms in the first several layers from their equilibrium positions leads to the compressive stress inside the film. Meanwhile, this deviation can be locked up by adherence of the substrate for the first few layers of films.

When the islands on the film continue to grow and are about to contact to each other, the energy released by reduction of surface area could drive the deformation of these islands to close the gap as shown in figure 3.3.

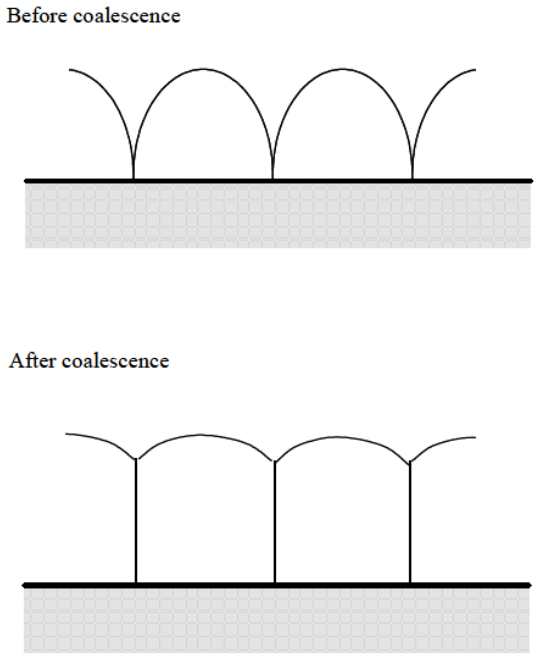


Figure 3.3. Crystallite coalescence (zipping) process[2]

At the end of the second stage, the tensile stress will decrease and become compressive. Eventually, the compressive stress will come to a steady value depending on the temperature and the depositing system. In sputtering deposition, the energetic atoms will bombard on the growth surface. This “atomic peening” process can generate plenty of excess interstitials in the near surface region. From the point view of thermodynamics, there is a tendency for the crystal to expel excess atoms at equilibrium conditions. What is more, the excess atoms at the boundary will also create a compress stress in the film. In the DLC film, the solid $sp^3$ bonds make it hard for the excess interstitial to move or diffuse to their equilibrium position, leaving an ultrahigh intrinsic stress inside the DLC film. Besides, argon atoms entrapped in the films might also play a role to raise the compressive stress in the film.

### 3.1.3. Me-DLC coating

It is hard to grow thick pure DLC film by PECVD as it introduces ultra-high residual stresses in the sputtering process because of the reasons preceding in this chapter. As shown in chapter 1, doping metal elements in the DLC film will decrease the film inside film.

It is reported that the metal element in the metal doping DLC film (Me-DLC) existed as metal carbide and presented a columnar structure[15, 45]. An example of the columnar structure is shown in figure 3.1.4.

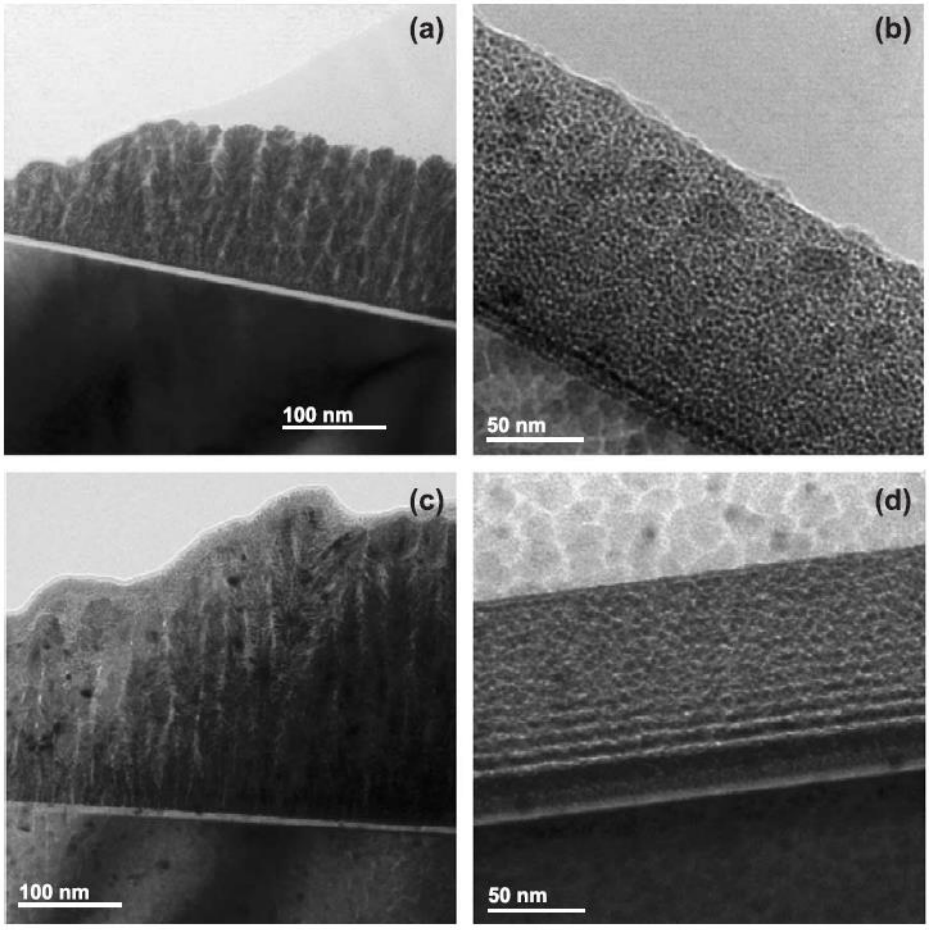


Figure 3.4. Cross-section TEM micrographs in the films:(a) W-DLC with 75 at.% W; (b) Mo-DLC with 30 at.% Mo; (c) Nb-DLC with 8 at.% Nb; (d) Ti-DLC with 25 at.% Ti [3]

These columnar structures throw some light on the mechanisms of how metal elements decrease the residual stress in the DLC film. The columnar structure divides the film into many small regions and prevent the residual stress passing though columnar structure. Therefore, it will be more difficult for the residual stress to accumulate into high enough to produce a crack, working the same mechanism as fiber strengthening.

### 3.2. Deposition of Cr-C:H film

DLC film was deposited by a hybrid CVD/PVD system, which combined an inductively coupled plasma (ICP) with magnetron sputtering. Details about this system has been discussed in chapter 2.

In a typical DLC film deposition, four steps were performed, i.e., sample preparation, plasma etching, Cr deposition, DLC deposition. Silicon wafer or commercial 316 stainless steel (SS316) plate were used as substrates. If a 316 stainless steel substrate was used, it will be polished by a series of sandpapers from 120 grit to 1200 grit in steps of 200 grit and then polished with diamond powders with radius of 6um, 3um, 1um in sequence. Both silicon wafers and SS316 plates were ultrasonically cleaned by deionized water, acetone, and ethanol. The sample was mounted to an aluminum plate and spined at a rate of 10 rpm controlled by a stepping motor.

The vacuum chamber was first pumped down to the pressure below $1\times10^{-7}$ Torr before deposition. To save time in the pumping process, the system might be baked by two heating tapes with the highest temperature not exceeding 80 $^{o}C$. After the pressure was pumped down to this level, a plasma etching process was performed to clean the sample first. In this plasma process, 50 sccm argon gas was let into the chamber. The pressure of the chamber was kept at 5 mTorr controlled by a gate valve. The ICP power was held at total 1000W (500W x 2). A bias (-100V for silicon and -50V for SS316 plate) was added to the substrate. The total plasma cleaning time is 10 min.

Following the plasma cleaning process, a chromium interlayer was deposited. 50 sccm agon gas was injeted into the chamber. The pressure of the chamber was kept at 5 mTorr controlled by a gate valve. The ICP power was held at total 1000W (500W x 2). A bias of -50V was added to the substrate. Meanwhile, a magnetron sputtering process was performed to deposit Cr interlayer. The Cr cathode current was kept at 0.5A during the deposition. The deposition time is 10 min.

Finally, a DLC film deposition was performed. 50 sccm argon gas and 5 sccm acetylene gas mixed by a tee joint at first and then the mixed gas was let into the chamber. The pressure of the chamber was kept at 5 mTorr controlled by a gate valve. The ICP power was held at total 1000W (500W x 2). A bias of -150V was added to the substrate. Meanwhile, the magnetron sputtering process was turned on to dope Cr element into the film. The Cr cathode current varied in the range of 0.2-0.5 A to get different content of Cr element in the DLC film.

As shown in table 3.1, a series of experiment have been taken to prepare high quality DLC films for the following micro-mechanical tests. Ratio of argon and acetylene, Cr target current, pressure, bias voltage, and depositing time have been investigated. Note that these parameters do not affect the process of DLC growth process independently. They work together to affect the energy of atoms arriving to the growth surface and the free energy of atoms at the surface or boundaries. Thus, the previously optimized parameter might be checked again after optimizing the one parameter.

Table 3.1. Different conditions to deposit the DLC film

| | Sample | Argon (sccm) | Acetylene (sccm) | Bias (V) | Cr current (A) | Pressure (mTorr) | Time (min) |
|---|---|---|---|---|---|---|---|
| Ratio of argon and acetylene | DLC028 | 50 | 3 | -100 | 0 | 5 | 30 |
| | DLC029 | 50 | 5 | -100 | 0 | 5 | 30 |
| | DLC035 | 50 | 3 | -150 | 0.2 | 5 | 60 |
| | DLC036 | 50 | 5 | -150 | 0.2 | 5 | 120 |
| | DLC051 | 50 | 7 | -150 | 0.2 | 5 | 120 |
| | DLC094 | 50 | 6 | -150 | 0.2 | 5 | 120 |
| | DLC096 | 50 | 8 | -150 | 0.3 | 5 | 60 |
| Cr current | DLC012 | 50 | 5 | -50 | 1 | 5 | 30 |
| | DLC013 | 50 | 5 | -50 | 0.5 | 5 | 30 |
| | DLC014 | 50 | 5 | -50 | 0.3 | 5 | 30 |
| | DLC015 | 50 | 5 | -50 | 0.1 | 5 | 30 |
| | DLC016 | 50 | 5 | -50 | 0.2 | 5 | 30 |
| | DLC036 | 50 | 5 | -150 | 0.2 | 5 | 120 |
| | DLC124 | 50 | 5 | -150 | 0.3 | 5 | 120 |
| Pressure | DLC021 | 50 | 5 | -50 | 0.3 | 10 | 90 |
| | DLC070 | 50 | 5 | -150 | 0.2 | 2 | 120 |
| Bias | DLC064 | 50 | 5 | -200 | 0.2 | 5 | 120 |
| | DLC065 | 50 | 5 | -120 | 0.2 | 5 | 120 |
| | DLC073 | 50 | 5 | -100 | 0.2 | 5 | 120 |
| Depositing time | DLC023 | 50 | 5 | -50 | 0.5 | 5 | 90 |
| | DLC048 | 50 | 5 | -150 | 0.2 | 5 | 240 |
| | DLC049 | 50 | 5 | -150 | 0.2 | 5 | 360 |

3.3. Results and discussion

3.3.1. Gas flux

Acetylene gas acts as the carbon source in the process of depositing DLC films. Argon gas is the working gas in the PECVD system. It will be ionized by the electromagnetic field generated by the two copper coils. The ratio of argon and acetylene gas flux plays an important role to determine how much degree of the acetylene is dissociated into carbon ions or carbon-hydrogen radicals.

As shown in figure 3.3.1 and figure 3.3.2, the two DLC films were deposited without doping Cr in the film. The ratio of argon and acetylene flux of the sample DLC028 is 50:3 while that of the sample DLC029 is 50:5. At a short depositing time (30min) and thin thickness (162nm and 381nm respectively), their surface is rough. Even there are big particles on and beneath the surface of the sample DLC029 when the acetylene flux increase. DLC028 film has a film growth speed of 5.4 nm/min and DLC029 has a film growth speed of 12.7 nm/min. The growth speed increased when the percentage of acetylene in the mixture gas increases. This is because there will be more carbon sources for film growth with more acetylene gas inlets into the chamber at the constant plasma generating power rate.

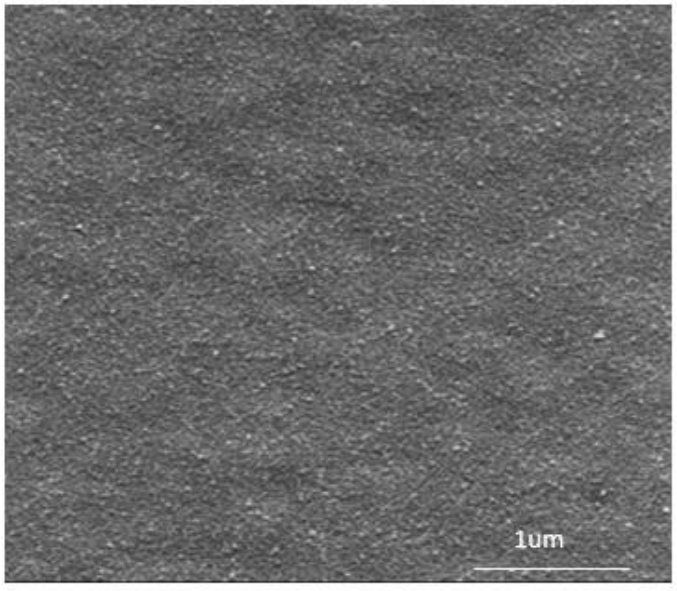


Figure 3.5. A SEM image of sample DLC028 deposited at 3 sccm acetylene with stage tilt at 52$^{o}$.

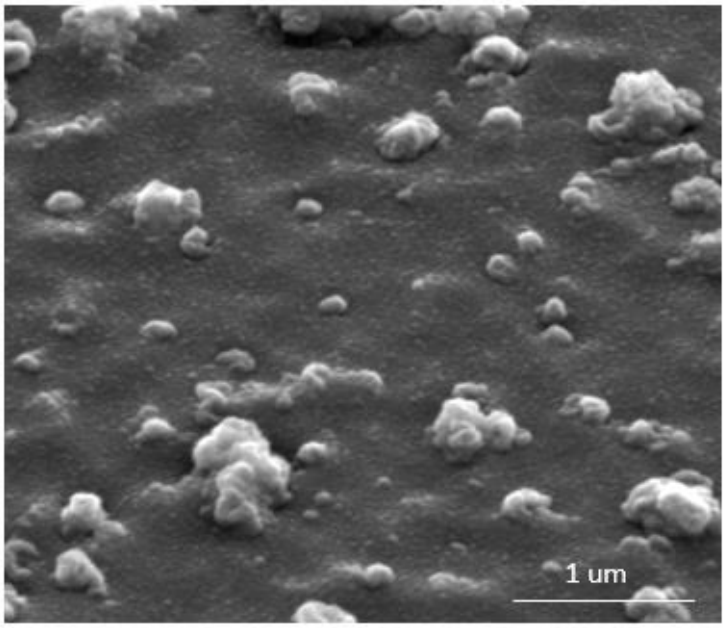


Figure 3.6. A SEM image of sample DLC029 deposited at 5 sccm acetylene with stage tilt at 52º.

Further, when the bias voltage increased and Cr element was doped into the film as shown in figure 3.3.3 and figure 3.3.4, it can be found that the big particles on the surface disappeared, and the surface was smooth even with longer depositing time by comparing the sample of DLC028 and DLC035 or comparing the sample of DLC029 and DLC036 under the same ratio of argon and acetylene gas flux. The film growth rate of the sample DLC035 is 1.75 nm/min and the film growth rate of the sample DLC036 is 10.8 nm/min. The film growth speed of the DLC films deposited at the bias of 150V decreased compared to that of the DLC films deposited at 50V.

The surface of the sample DLC035 and DLC036 seems all provide a smooth surface and dense film. But the DLC035 has a so low film growth rate that if we want to deposit a thick film say 2 um, it will take too much time (about19 hours) to do the deposition. Meanwhile, as we have talked in chapter 3.1, if there are more argon atoms than carbon atoms in the chamber, the “atomic peening” effect may increase the residual stress inside the DLC film. Besides, argon atoms will be more likely to be trapped inside the film and the trapped argon atoms will increase the residual stress in the DLC film too. Figure 3.3.5 shows the cross-sectional SEM image indicating that the film of sample DLC036 is dense.

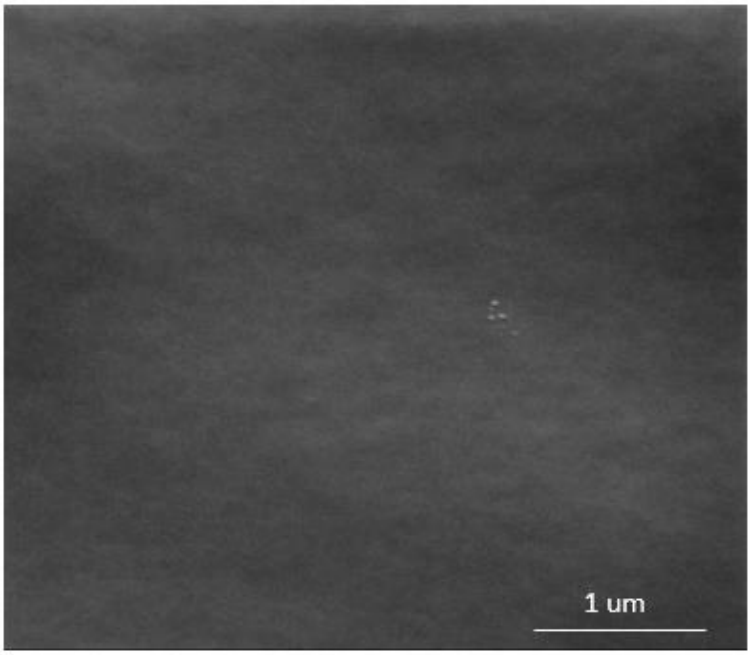


Figure 3.7. A SEM image of sample DLC035 deposited at 3 sccm acetylene with stage tilt at 52$^{o}$.

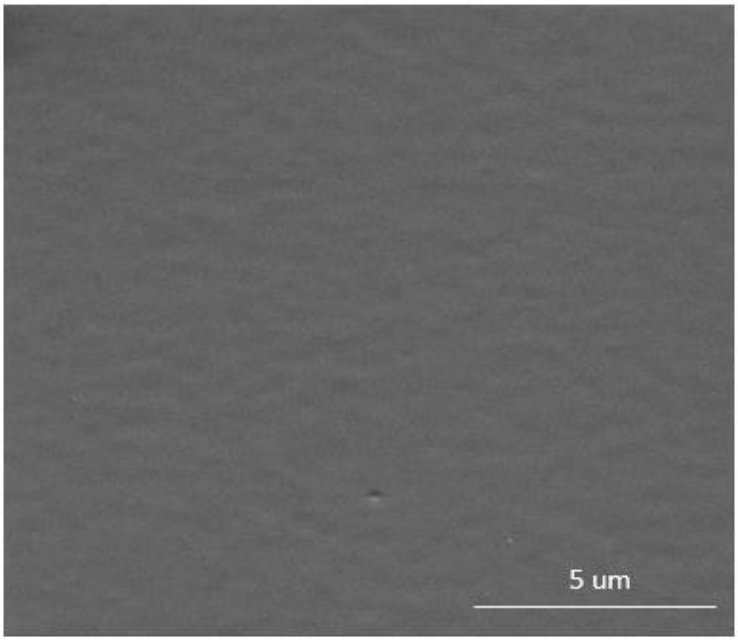


Figure 3.8. A SEM image of sample DLC036 deposited at 5 sccm acetylene with stage tilt at 52$^{o}$.

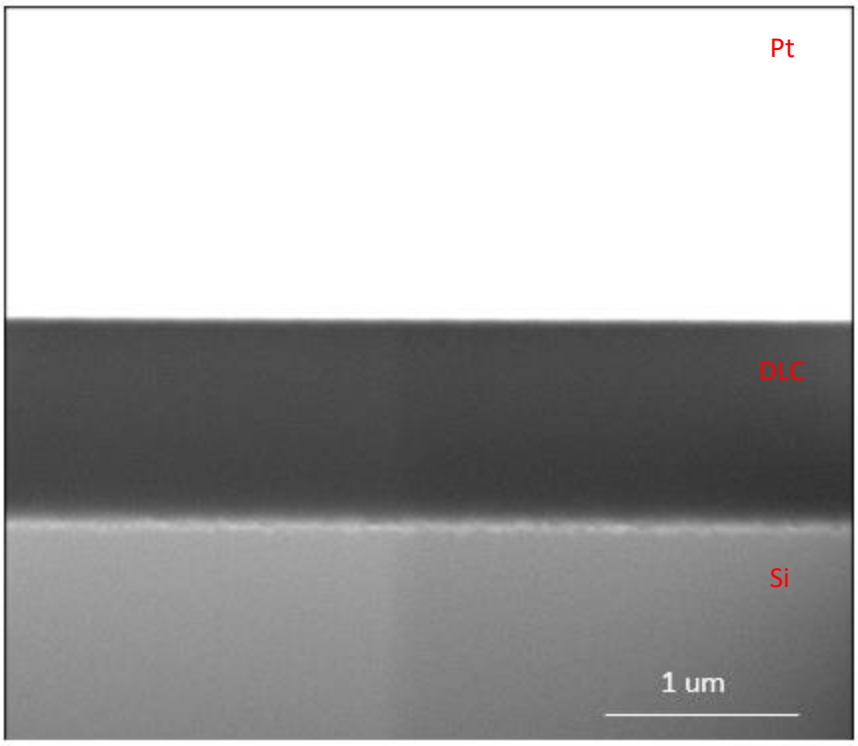


Figure 3.9. A Cross-sectional SEM image of the sample DLC036.

In a PECVD system, the argon atoms will be ionized into argon ions and electrons by the electromagnetic field. When a negative potential is added to the substrate, argon ions generated in last step will be attracted to move forward to the substrate and bombard the surface with a kinetic energy of the potential gap between the plasma and the substrate. If one or more argon ions crashes into an acetylene molecule, the acetylene molecule would be dissociated into carbon-hydrogen radicals. The acetylene flux will affect how much acetylene is available in the chamber to be utilized for carbon source. The ratio of the argon and acetylene gas fluxes will affect the degree of acetylene dissociation by argon ions at a constant plasma generating power rate hence determines the final number of carbon atoms that can be obtained to deposit at the substrate. Meantime, the bias voltage will determine how much kinetic energy of the carbon atoms (or carbon-hydrogen radicals) and argon atoms when they bombard at the surface of the substrate. If the bias voltage is too low, the carbon atoms might not have enough energy to move around the surface and stuck at the position where they arrive at the surface initially. Finally, there will be some unexpected particles formed on the film surface. On the contrary, if the bias voltage is too high, Most of the carbon atoms or carbon-hydrogen radicals still have enough energy to leave the surface again after they attach to the surface. Meantime, the high argon ions will also bombard at the film surface and show a plasma etching effect. As a result of the two factors, the film growth speed will decrease.

When the percent of acetylene in the argon and acetylene mixture gas increases to get a higher film growth rate, spallation occurred in the DLC films (DLC051 and DLC094) deposited at 50:7 and 50:6 of argon and acetylene flux ratio. A SEM images at the edge of spallation was

shown in Figure 3.3.6. The reason of spallation can be that the acetylene molecules are more likely to be broken down into carbon-hydrogen radicals rather than carbon atoms. Thus, these films contain more hydron atoms which decrease the strength of the film as these hydrogen atoms acts as a terminator in the carbon network structures. But when the ratio of argon and acetylene gas flux increases to 50:8, the film didn't spall but had many big particles on the surface as shown in figure 3.3.7. The possibility for carbon atoms to meet each other to produce a cluster before arriving at the substrate increases when the acetylene percentage increase. By cutting a cross section on the DLC film by FIB, some of these big particles passes through all the DLC film to the substrate. These particles prevent the residual stress from accumulating to a level of producing a crack in the film.

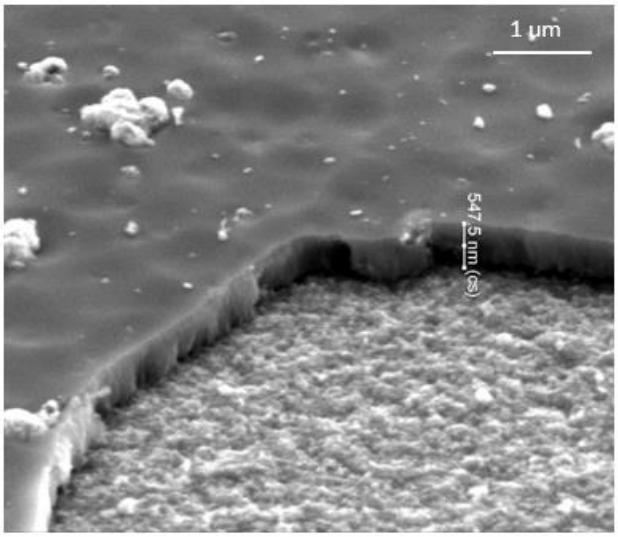


Figure 3.10. A SEM image of sample DLC094 deposited at 6 sccm acetylene with stage tilt at 52º.

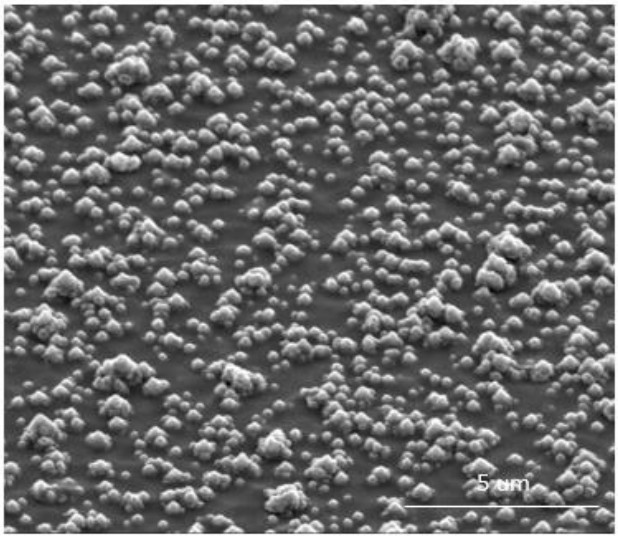


Figure 3.11. SEM images of sample DLC096 deposited at 8 sccm acetylene with stage tilt at 52º.

With the discussion above, the 50:5 ratio of argon and acetylene should be the best choice in these conditions. It provides a smooth surface and dense film with no particle on the surface. A higher percentage of acetylene in the mixture gas will increase the possibility of carbon atoms to produce clusters before arriving at the substrate and form big particles on the surface. On the contrary, a lower percentage of acetylene in the mixture gas will decrease the film growth rate a lot, making it most impossible to deposit a film in practice.

### 3.3.2. Cr cathode current

Metal elements exist inside the DLC mostly in the form of metal carbides. As shown in the previous chapters, doping metal element in the DLC film will decrease the residual stress. But it is still not fully understood by what mechanism the metal elements use to reduce the residual stress in the DLC film. In this experiment, different concentrations of Cr element were doped inside the DLC film to decrease the residual stress inside the film and obtained a good enough DLC film for the following experiment.

The Cr element concentration in the DLC film was controlled by the Cr target current in the magnetron sputtering process. A series of Cr target current of 1.0A, 0.5A, 0.3A, 0.2A were used to deposit the DLC film. The results were shown in the figure 3.3.8-11 respectively. Spallation occurred in the sample DLC015 deposited at 0.1A Cr target current and no SEM images was taken for that sample.

The film of sample DLC012 deposited at 1.0A was porous. EDS results show it contains 70.6 at. % Cr element. This indicates that Cr element in this film exists as Cr atoms and chromium carbide. And carbon atoms mostly exist in the form of carbide. When the Cr target current decreased to 0.5A, A dense Cr-DLC film was obtained but with a rough surface. EDS results shows it contains 26.9 at.% Cr element. Note that the Cr concentration in the Cr-DLC film is not a linear function of Cr target current. When the Cr target current continued to decrease to 0.3A, the film seems to be smooth but with some big particles on the film. As we discussed in chapter 3.3.1, these big particles should be because of the low bias voltage. When the Cr target current decreased to 0.2A, there were more big particles on the surface of DLC film. Here we notice that when the doped Cr element is low, the Cr-DLC film behaves close to the pure DLC film and carbon atoms tend to form big particle. When increasing the concentration of Cr element in the film, it will get a smoother surface with less big particles. With a high Cr concentration in the film, it will have a wider window to get a better film if other depositing parameters are not optimized. Compared the results of sample DLC029 and sample DLC016, we assume that the low bias voltage causes these big particles as there are less big particles on the surface of sample DLC029 than DLC016 although DLC029 contains no Cr element at all but with a high bias voltage of deposition.

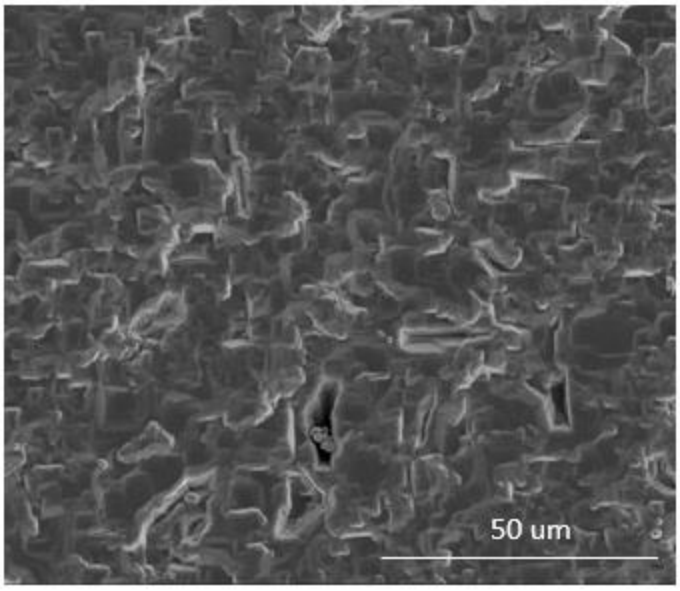


Figure 3.12. A SEM image of sample DLC012 deposited at 1.0A Cr current.

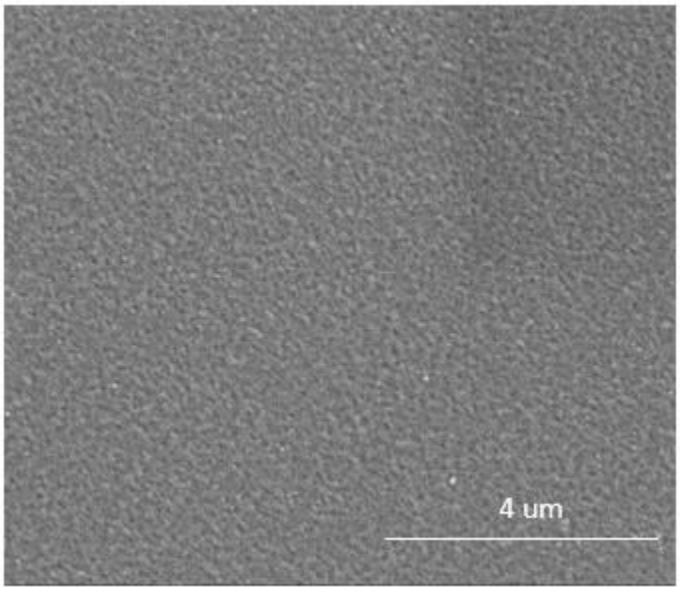


Figure 3.13. A SEM image of sample DLC013 deposited at 0.5A Cr current.

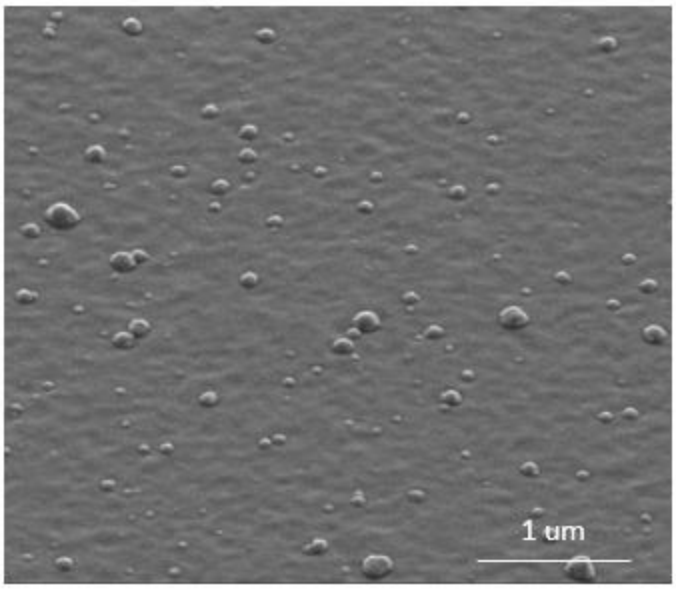


Figure 3.14. A SEM image of sample DLC014 deposited at 0.3A Cr current.

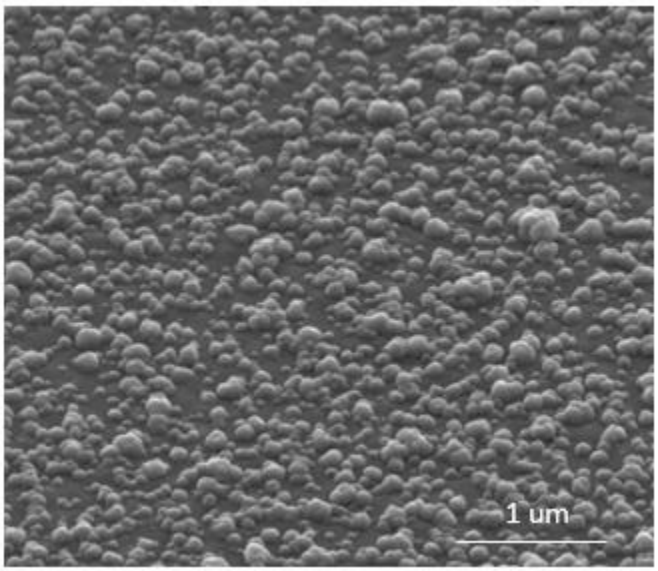


Figure 3.15. A SEM image of sample DLC016 deposited at 0.2A Cr current.

To check this assumption, the bias voltage was increased to -150V while other conditions keep the same with sample DLC016. The result was shown in figure 3.3.12. By adding a higher voltage, the big particles on the surface of DLC films disappeared. The surface of the film was smooth. DLC124 is another sample that can prove this relationship between the big particles and the bias voltage. It was deposited at -150V bias voltage and keep other depositing parameters the same with the sample DLC014. A SEM image of DLC124 was shown in the figure 3.3.13

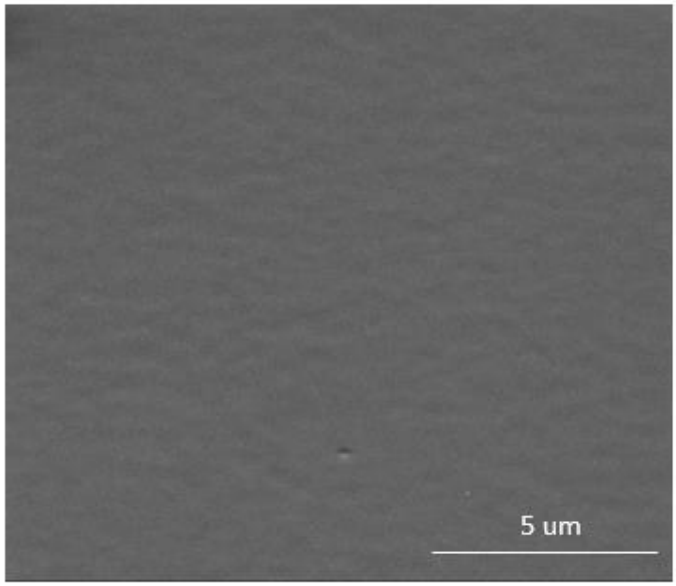


Figure 3.16. A SEM image of sample DLC036 deposited at 0.2A Cr current with stage tilt at 52$^{o}$.

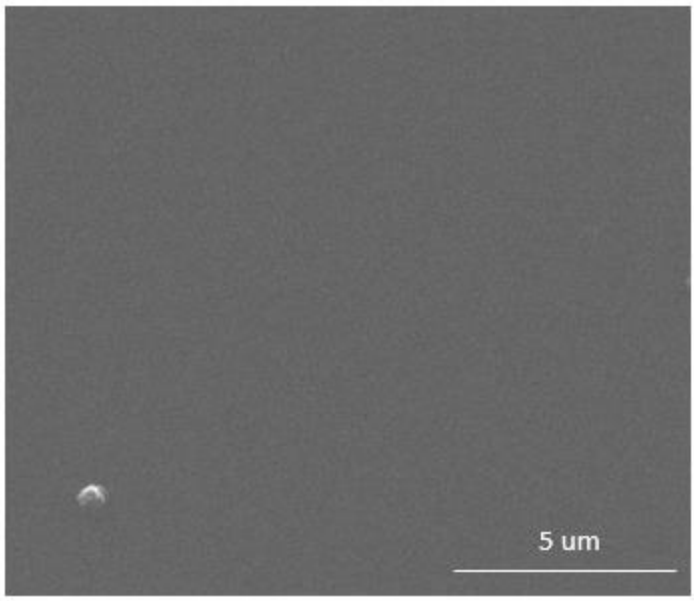


Figure 3.17. A SEM image of sample DLC124 deposited at 0.3A Cr current.

3.3.3. Pressure

Pressure will determine how many atoms will distribute in a unit volume inside the chamber. Although the DLC process in the chamber is not an equilibrium process, the deviation of the chamber pressure to the saturation pressure of the film materials will affect the free energy of the adatoms on the growth surface, even affect the distribution of different element in the film. Different depositing pressures of 10 mTorr, 5 mTorr, 2 mTorr are checked at different period of the experiment. The chamber pressure was controlled to the set value at the beginning of film deposition by a gate valve. The real pressure of the chamber will increase a bit (one or two mTorr) because of temperature of the chamber increasing with depositing time. At constant gas flux into the chamber and the constant pumping rate of the turbo pump, the cause of pressure increase are assumed to be because of the temperature increase of the temperature of gas molecules. But the gas atomic density inside the chamber is steady. The chamber pressure during all the film depositions in this thesis of the time were not controlled intentionally.

Sample DLC021 was deposited at 10 mTorr, and sample DLC014 was deposited at 5 mTorr. Other parameters of these two samples were the same. As shown in figure 3.3.14, the film is not dense, and its surface is not smooth. It has more and bigger particles on the surface than the sample DLC014.

Sample DLC070 was deposited at 2 mTorr, and sample DLC036 was deposited at 5 mTorr. Other parameters of these two samples were the same. Sample DLC070 didn't show a film but many black powders on its surface after deposition. When removing the powders with dust-free papers, a film was found below these black powders. A SEM images of this film was shown in figure 3.3.15. It indicates that at first there is a DLC film formed on the substrate with a bad quality. When it grows along time, the film becomes worse and worse and finally it turns into powders.

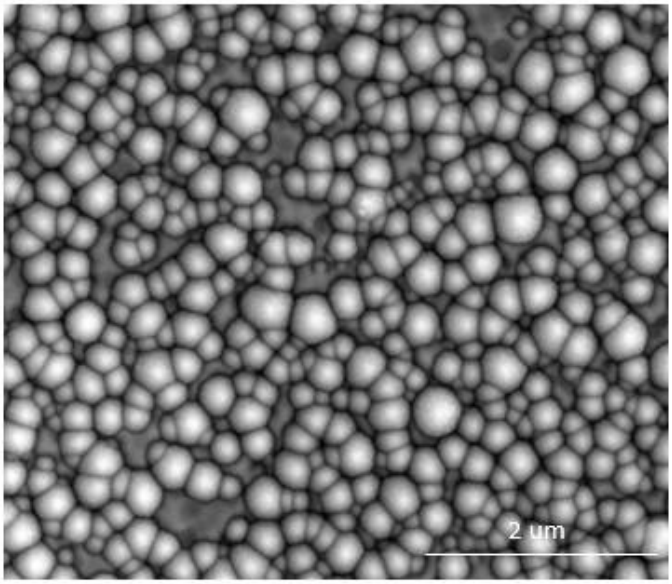


Figure 3.18. A SEM image of sample DLC021deposited at the pressure of 10 mTorr.

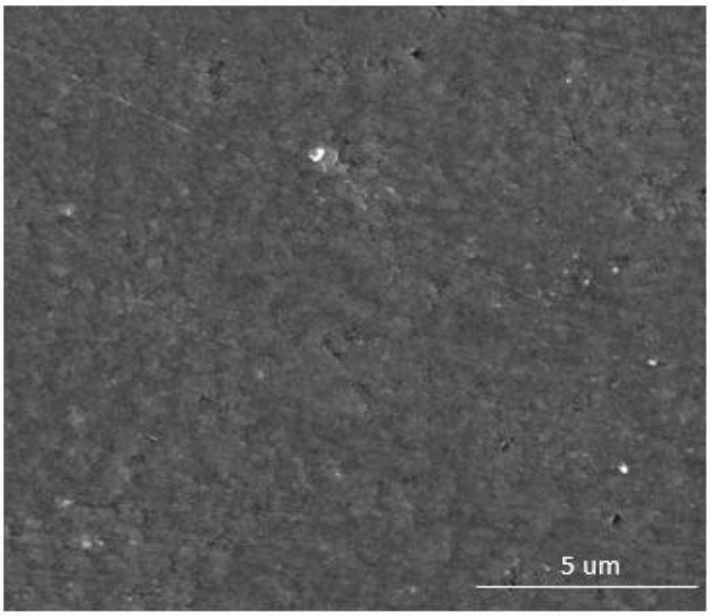


Figure 3.19. A SEM image of sample DLC070 deposited at the pressure of 2 mTorr.

Both sample DLC036 and sample DLC014 deposited at 5 mTorr have shown a good quality of DLC film. Pressure higher or lower than this pressure will decrease the quality of the DLC or have no film at all. A closer examination of the pressure around 5 mTorr might be meaningless at the fluctuation of the chamber pressure during the deposition along time.

### 3.3.4. Bias voltage

The effect of bias voltage has been discussed much in the previous parts of the same chapter. Besides the bias voltage of 50V and 150V, other bias voltages of -100V, -120V and -200V were also checked. DLC films deposited at -100V (sample DLC073) and -120V (sample DLC065) were similar to the results of sample DLC070. There was a layer of powders on the surface while a film beneath the powder layer. If the depositing time was short, say 30min, there should be seen a film deposited on the substrate. But the quality of the film is bad. When the film continues to grow on the bad film base, it develops to worse surface and finally turns to powder. No SEM images was taken for these samples. Sample DLC064 was deposited at the bias voltage of 200V. The surface is not smooth. And many small spallation areas have already existed on the surface, indicating that film deposited at this condition has a higher residual stress. Compared to the results of sample DLC036 and sample DLC124, 150V is a better choice for the bias voltage.

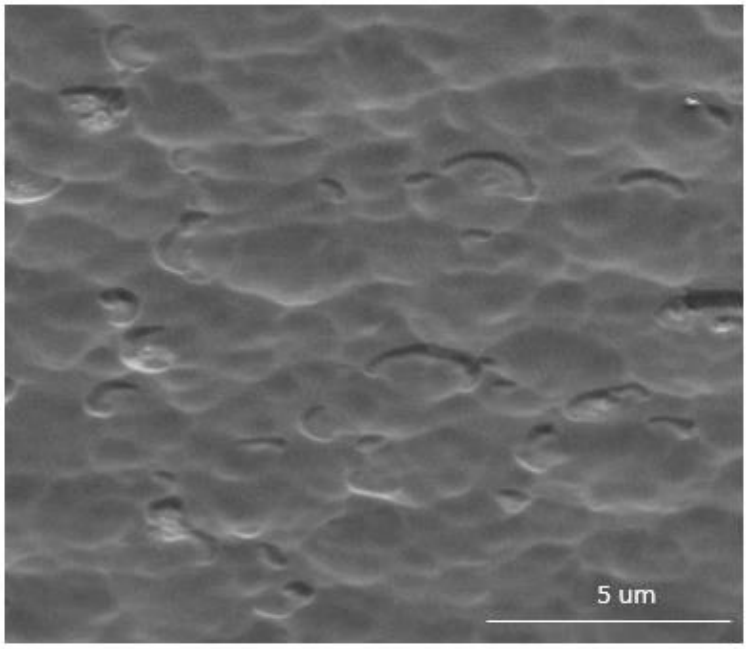


Figure 3.20. A SEM image of sample DLC064 deposited at -200 bias voltage with stage tilt at 52$^{o}$.

3.3.5. Depositing time

When the DLC film grows thicker, the growth surface will move away from the surface of substrate gradually. Thus, a deviation of some parameters is inevitable. For example, the resistance of the DLC film will increase as the thickness of DLC film increases during film growth. Hence, the bias voltage will also change a bit during the film growth. The temperature at the growth surface faces the same situation with bias as it becomes harder for the film to transport heat in thicker DLC film. What is more, the residual stress in the DLC film increases when the film thickness increases. High residual stress might result in small spallation on the surface. If a defect occurs on the DLC film, the following film depositing process will keep this defect, if not developing it since the depositing condition at the defect is not the same with other parts and is not as expected.

As shown in figure 3.3.17, there are many small holes and some particles on the surface of sample DLC023, which was deposited for 90 min. Sample DLC013 was deposited at the same condition with sample DLC023, but its depositing time is 30 min, the surface of which was shown in figure 3.3.9. The surface of sample DLC013 is rough and can be seen as many smaller holes on it. When the film continues to grow, the small holes on the surface of sample DLC013 work as seeds to grow to bigger holes on the surface like in sample DLC023. The roughness of the surface becomes worse and worse as the later several layers of DLC film are based on the former layers. Finally with this process developing to a degree, the DLC film will turn into powders and no film

formed any longer. This phenomenon has been seen in sample DLC070, sample DLC065 and sample DLC073.

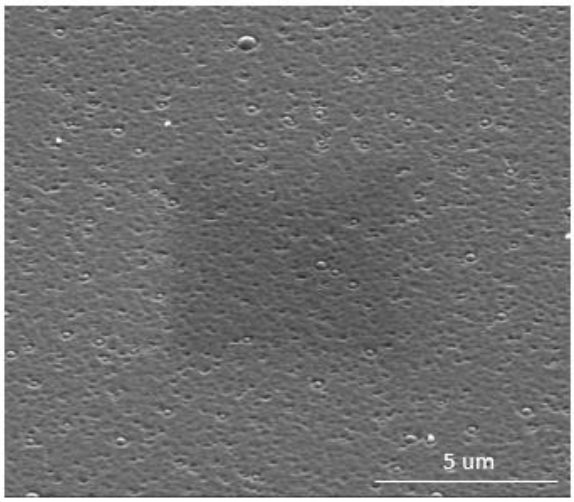


Figure 3.21. A SEM image of sample DLC023 deposited at 0.5A Cr current with stage tilt at 52°.

Sample DLC036 was deposited for 120 min (shown in figure 3.3.12). It has quite a smooth surface with no spallation and particles. But when the depositing time increases, holes and particles exist on its surface. Sample DLC048, which was deposited for 240 min, has a smooth surface in most regions except some holes and particles as shown in figure 3.3.18. When the depositing time is longer, more holes and particles occur on the surface, as shown in figure 3.3.19 for sample DLC049, which was deposited for 480 min. But the surface is smooth in other regions except of the holes and particles. This indicates that the film can be grown smooth for thicker by long time deposition if there are no holes to occur in the film, not like what have happened to the sample DLC023.

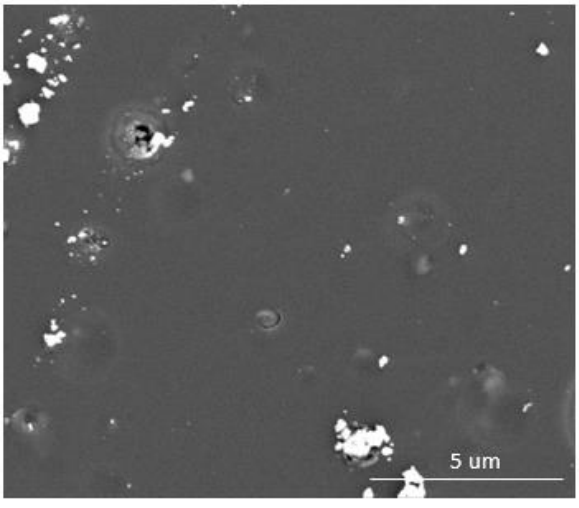


Figure 3.22. A SEM image of sample DLC048 deposited for 240 min.

A cross-sectional SEM image is shown in figure 3.3.20. A small spallation occurred at the top of the film. And these holes seem to be distributed on the surface in a random way. That gives us some idea for what happened to these holes. These holes on the surface should originate from the small spallation during the deposition. If the time to produce these holes is close the end of deposition, then we will see a hole on the surface. But if these holes were produced earlier, big particles would be formed as the deposition condition changed as a result of the hole. However, as we can see there almost no holes or particles were seen for the first 120 min in sample DLC036, it can be judged that these holes are not through the film.

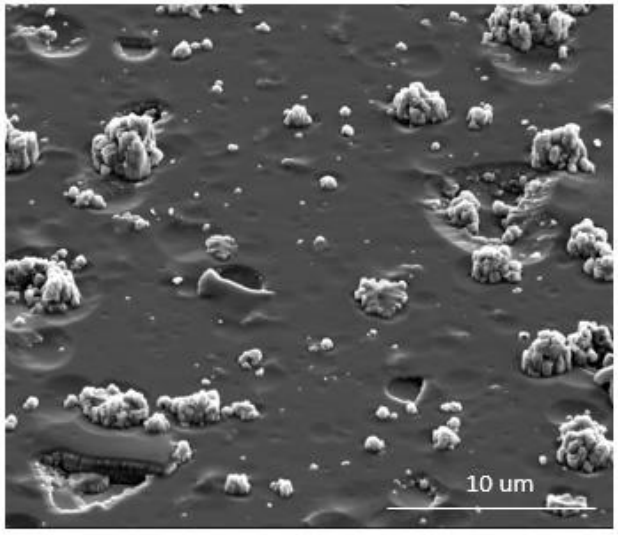


Figure 3.23. A SEM image of sample DLC049 deposited for 360 min.

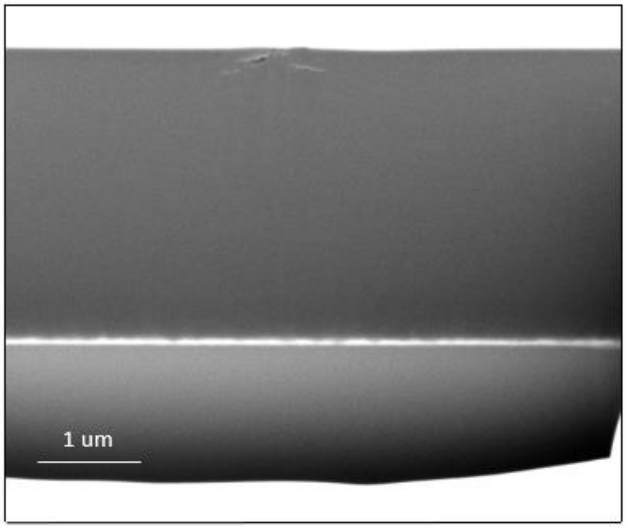


Figure 3.24. A cross-section SEM image of sample DLC049 deposited for 360 min.

One of the important applications of DLC film is as a protective coating on substrates, for example steel. Now we have got an optimized condition to deposit DLC film on silicon wafer. Figure 3.3.21 shows the results of DLC124 deposited on silicon with the same condition of DLC036 with a depositing rate of 9.4 nm/min. So next step of this work is to transfer the substrate of DLC film from silicon wafer to SS316 plate. Generally, there is an Cr interlayer between DLC and substrate. DLC films should have no preference for the substrate, provided that a Cr interlayer can be deposited on that substrate first. But deviation still can happen because of the thickness of the substrate or something unknown.

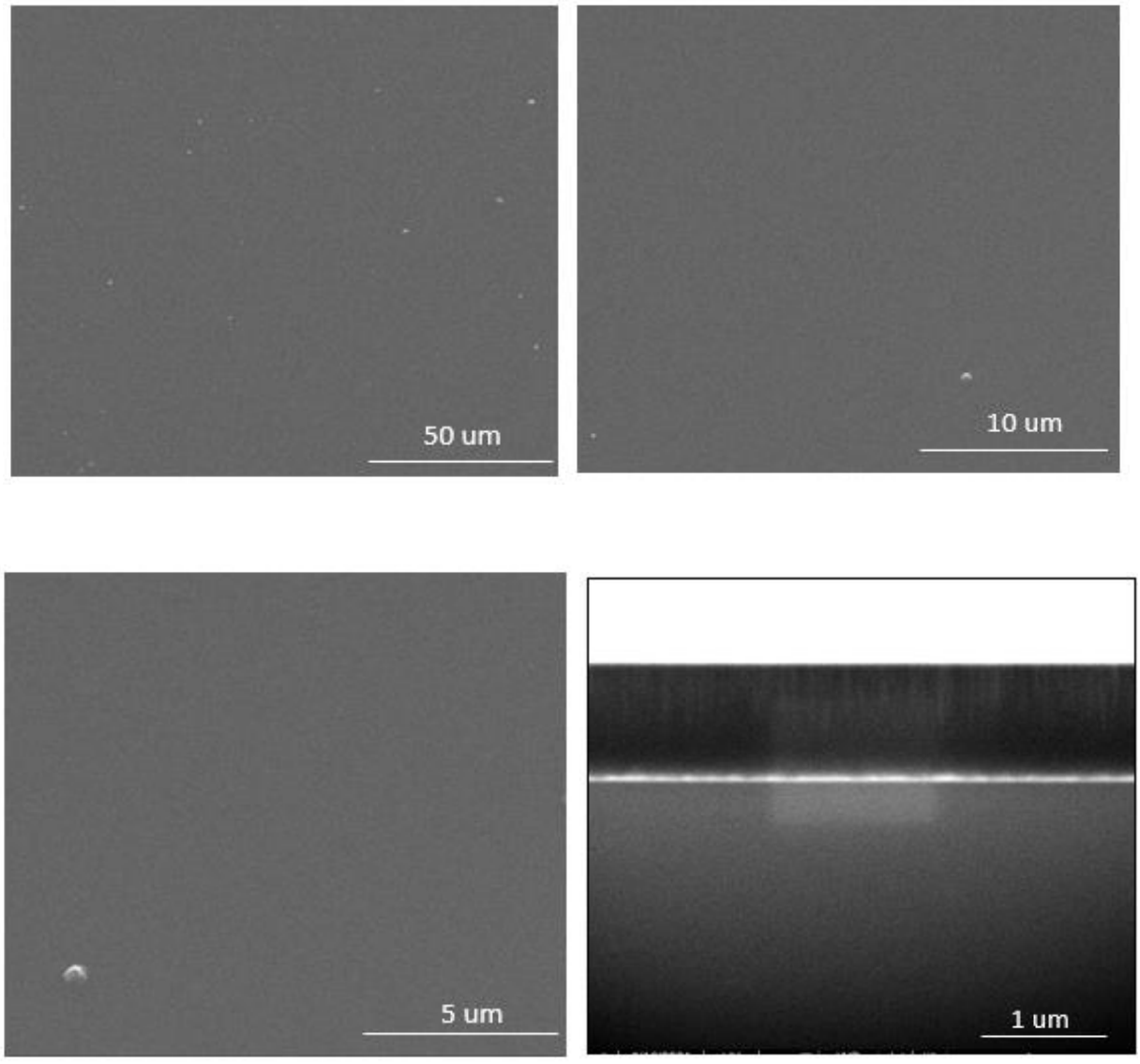


Figure 3.25. SEM images of sample DLC124 on silicon wafer.

A typical cross-sectional image deposited under the same condition with DLC124 but on the SS316 steel plates is shown in figure 3.3.22. Some adjustments should be done to the deposition parameters before depositing DLC film on SS316 plates. Compared to Figure 3.1.4, the deviation of depositing condition has caused the film to grow with obvious columnar growth. And also there is a different phase between the DLC film and the SS316 plate. The geometry of the plates and thermal and electrical properties of SS316 steel might work together to cause this problem. But the surface of the film was smooth indicating that the condition to deposit DLC layer still works on SS316 substrate.

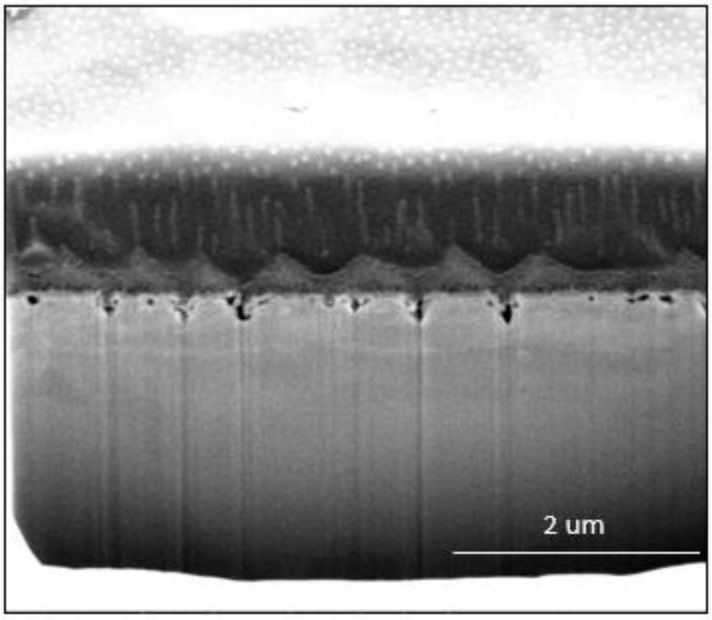


Figure 3.26. A cross-sectional SEM image of DLC083 on SS316 steel plate.

To handle this problem, two modifications in the depositing process have been done. First, a bias voltage of -100V was used to clean the silicon substrate in the plasma etching process. But this high bias voltage will plasma etch the SS316 plate heavily. So, the bias voltage was decreased to -50V for SS316 substrate in the plasma etching process. Second, the Cr target current to deposit the Cr interlayer by magnetron sputtering was changed from 0.8A to 0.5A. After these two changes, a dense and smooth DLC film (sample DLC123) can be deposited on SS316 plates as shown in figure 3.3.23.

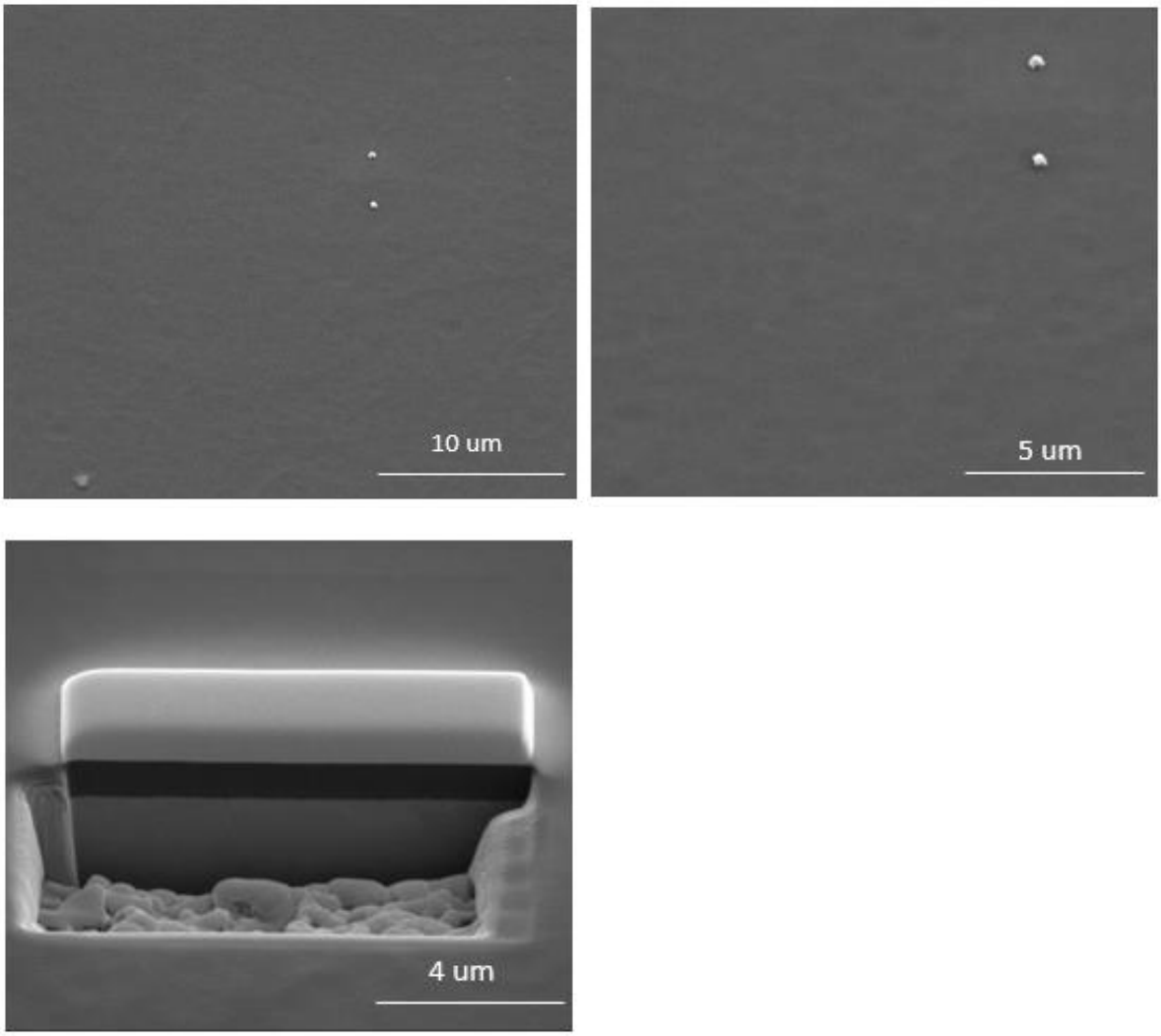


Figure 3.27. SEM images of sample DLC123 on SS316 plate.

The Young's modulus and hardness of sample DLC123 was tested by instrumented nanoindentation (Nano-Indenter$^{TM}$ XP, MTS), as shown in figure 23.3.23. Figure 3.3.24 shows the results for the Young's modulus and hardness of the DLC film as a function of indentation depth. There is an apparent hardness increase as the Berkovich indenter has a finite tip radius. When the indentation depth goes higher, the measured Young's modulus and hardness tend to the value of the substrate. The hardness reaches a peak of 5.7 GPa at the indentation depth around 306 nm (corresponding maximum load is 10 mN). And the corresponding Young's modulus measured at this depth is 90.2 GPa.

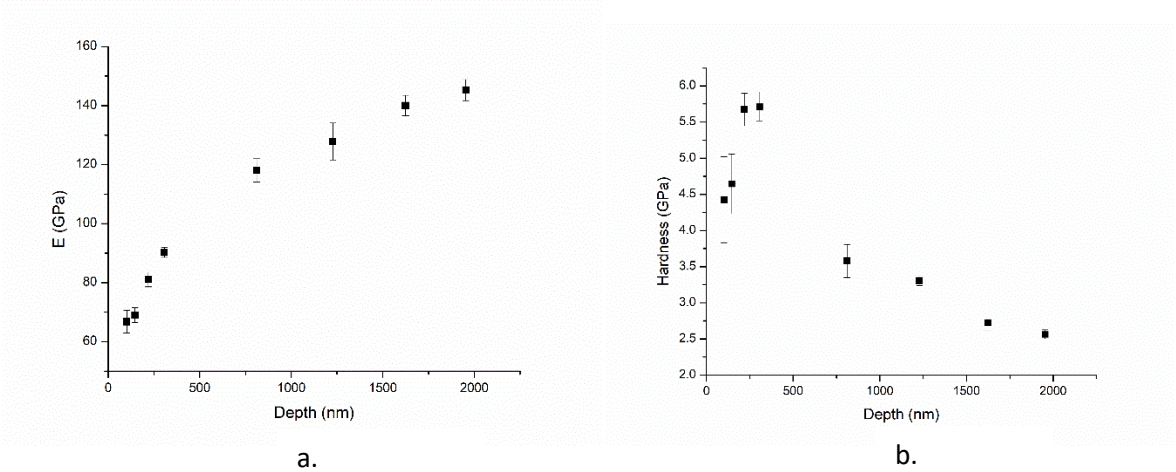


a. b.

Figure 3.28. a. Young's modulus vs. max indentation depth of sample DLC123; b. hardness vs max indentation depth of sample DLC123

## 3.4. Conclusion

In this chapter, we checked the depositing parameters of ratio of argon and acetylene gas fluxes, Cr target current, pressure, bias voltage, and deposition time and got an optimized condition to deposit Cr-DLC film on silicon wafer. Then we went on to do some adjustment to the deposition process to make it suitable to deposit DLC film on SS316 substrates. Last, we tested the properties of sample deposited at this condition, including nanoindentation test, corrosion test. Eventually, we prepared the sample to do the V-notched micro-beam test.

# Chapter 4. Multilayer DLC films and micro-mechanical testing

## 4.1. Introduction to multilayer films

DLC films have high residual stresses that spallation from the substrate will occur before the film thickness reaches hundreds of nanometers. Even by doping metallic elements into the DLC film, several microns thick DLC films can be difficult to obtain. There are a number of defects existing on the surface of thick films because of spallation. To deal with this problem, methods of multilayer film is a promising way to enhance the adhesion between DLC film and substrate and improve the quality of DLC films.

Multilayer films now have been widely investigated around the world to get new multifunctional thin films to provide superior mechanical, tribological, chemical, and high-temperature properties and performance [4]. Stuber et al. has reviewed the influence of the interface volume on the properties of nanoscale multilayer coatings as shown in Figure 4.1.1. From the figure, it can be found that the interface volume in the multilayer film effectively reduces the residual stresses in a linear way and it also increases the toughness when the interface volume is higher.

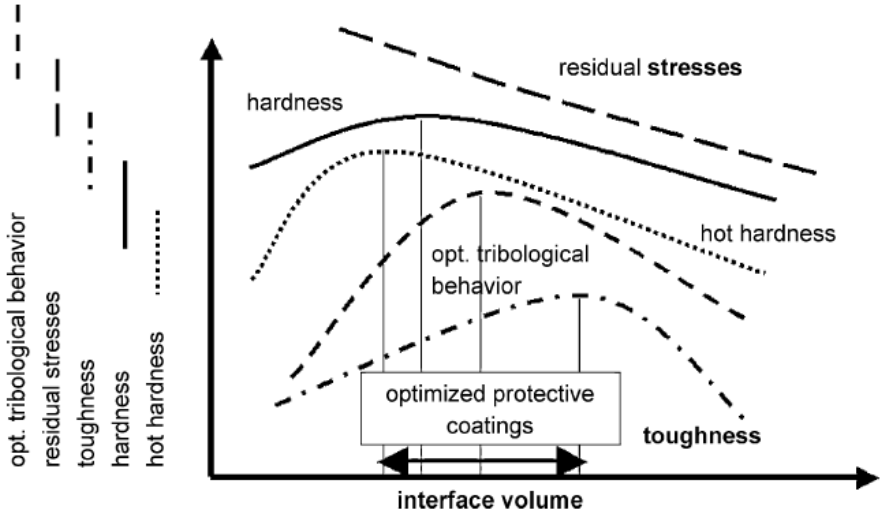


Figure 4.1. Change in properties of nanoscale multilayer coatings as a function of the interface volume (schematically, disregarding superlattice structures) [4].

Multilayer film methods can enhance the film in several ways at the same time. Stueber et al. concluded these strengthening and toughening mechanism in three aspects [4]. As shown in figure 4.1.2, first, when a mechanical load is added to the surface of a multilayer film, a crack starting from the surface may be blocked at the grain or phase boundary within a layer or at the interface between the layers. Second, local delamination might occur at the interface between different layers by producing nano-voids, which will relax the local stress. Third, there should be

an interaction between the cracks and the periodic strain-stress fields across the interfaces in nanoscale multilayers.

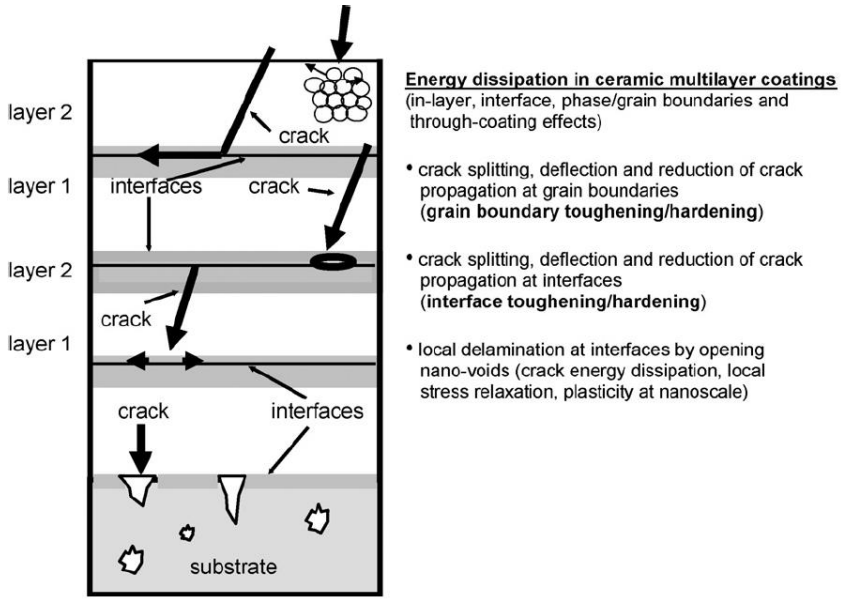


Figure 4.2. Toughening and strengthening mechanisms in ceramic multilayer coatings (schematically) [5].

When it comes to DLC films, the situation becomes more complicated. DLC films are amorphous. The multilayer structure not only affects the DLC film by the strengthening and toughening mechanism discussed above but also by affecting the growth process. The multilayer methods used in DLC film can be divided into two categories, compositionally graded films and layer-by-layer films (LBL). Compositionally graded DLC films have attracted much attention in the past decades by setting different substrate temperature, bias voltage, metal element doping concentration to deposit different DLC layers or to add a series of compositionally graded transitional interlayers [48–55]. Compositional gradient in thin film can eliminate abrupt transitions in thermal, elastic, and plastic mismatch at the interface and achieve strong adherence between the substrate and the film. It can also mitigate stress concentrations at the conners at sharp interfaces and can be used as buffer layers to manipulate dislocation densities and mobility in optoelectronic devices. What is more, spatial gradients in elastic and/or plastic properties could redistribute the contact stress during frictional sliding stress [1].

However, not much work has been done on the lay-by-layer method to deposit DLC films. Dwivedi et al. deposited a varied number of Ti/DLC bilayers from 1 to 4, and checked their mechanical properties by nanoindentation along with their optical and electrical properties [56]. The layer-by-layer method can be expected to have many advantages that it has relatively sharp interfaces between different layers. The crack front can be blocked at these sharp interfaces. Also, as discussed in chapter 3.1, there are different stages at the beginning of DLC film growth process. The stress can be compressive or tensile at different stages. Meanwhile, if the process was

disrupted by a pure metal layer, the growth process will restart again. Hence, there will be several different stress regions with compressive or tensile stresses in the DLC film deposited by the LBL method, dividing the films into different smaller layers according to their residual stresses. In such a way, the residual stresses in the DLC film can be localized and limited to a smaller level. What is more, the metallic carbides in the DLC film have a columnar structure as shown in Figure 3.1.4. These pure metal layers together with these columnar structures of metallic carbides will form a complex network to strengthen the DLC film further.

In this work, we will prepare an alternating Cr/Cr-DLC multilayer film and test it by the V-notched microbeam method.

## 4.2. Depositing the Cr/Cr-DLC multilayer DLC films

Two samples of DLC film were deposited to do the test. One sample of DLC films is a single Cr/Cr-DLC bilayer. And the other one is three Cr/Cr-DLC bilayers. Both samples were deposited on commercial SS316 steel plates. These SS316 plates were polished from 200 grit sandpaper to 1200 grit sandpapers before polished by diamond powders with a diameter of 6 um, 3 um, 1um in sequence. After polishing, these SS316 plates were ultrasonic cleaned with deionized water, acetylene, and ethanol in sequence. Then these SS316 plates were dried by pure nitrogen gas before rinsed with pure ethanol again. Then these SS316 plates were mounted to an aluminum holder in the deposition system to deposit DLC film on them.

Then these substrates were cleaned by a 10 min plasma cleaning process after the pressure of the chamber was pumped down below $1x10^{-7}$ Torr. The whole chamber was baked by two heating tapes. During the plasma cleaning process, the bias was set to be -50V with a DC power source. The argon gas flux was set to be 50 sccm by a mass flowmeter. The pressure of the chamber was adjusted to 5 mTorr by a gate valve. The ICP power was set to 1000W (500W x 2) for all the three processes to deposit DLC films. The sample spined at a rate of 10 rpm during the plasma etching process.

Following was the Cr interlayer deposition process. In this process, the set up about the plasma generating system was the same with the plasma etching process. Then the magnetron sputtering system was turned on to deposit the Cr interlayer. Two Cr targets were mounted in this system. The Cr target current was set to 0.5 A. The thickness of the Cr interlayer for both films were estimated to be around 100 nm.

The last step was to deposit the DLC layer with the deposition condition of sample DLC124. To deposit the single Cr/Cr-DLC bilayer DLC film (sample DLC130), the bias voltage was adjusted to -150V. Acetylene gas was let into the chamber with a flow rate of 5 sccm. The depositing time is 180 min. A cross-sectional SEM image of sample DLC130 was shown in figure 4.2.1.

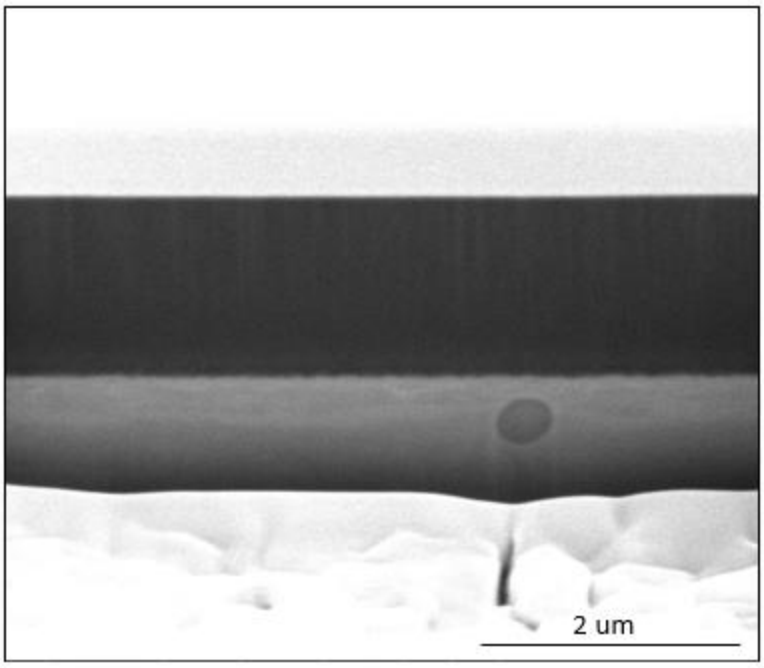


Figure 4.3. A cross-sectional SEM image of sample DLC130.

To deposit the three Cr/Cr-DLC bilayers DLC film (sample DLC132), the parameters were the same with that of sample DLC130 except that a 10 min Cr interlayer deposition was performed with the same depositing parameters to depositing Cr interlayer in the second step every 40 min. Repeat this procedure three times to get three DLC layers in the DLC films. A cross-sectional SEM image of sample DLC132 was shown in Figure 4.2.2.

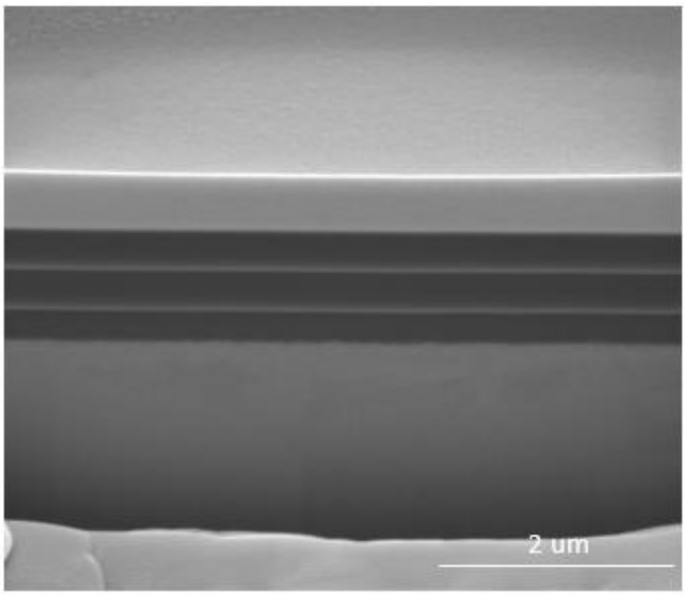


Figure 4.4. A cross-sectional SEM image of sample DLC134.

Young's modulus and hardness of sample DLC134 was tested with the same procedure at chapter 3.3. The results were shown in Figure 4.2.3. The measured hardness reaches a peak of 7.0 GPa at the indentation depth around 291 nm (corresponding maximum load is 10 mN). And the corresponding Young's modulus is 83.7 GPa. Compared to the single layer of sample DLC123, the hardness of DLC films with three Cr/Cr-DLC bilayers increases from 5.7 GPa to 7.0 Gpa while its Young's modulus decrease from 90.2 GPa to 83.7 GPa.

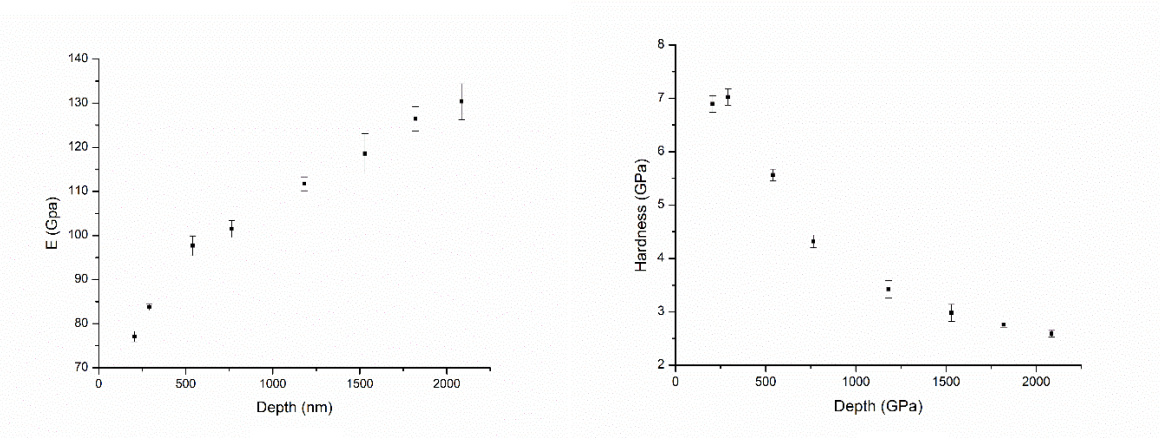


Figure 4.5. a. Young's modulus vs. max indentation depth of sample DLC134. b. hardness vs max indentation depth of sample DLC134

## 4.3. Testing method of fracture toughness

Bending test of a V-notched microbeam was performed to measure the mechanical properties of DLC films.

The notched microbeam was prepared by the focused ion beam system (FIB, FEI Quanta 3D FEG FIB/SEM Dual Beam System). The procedure was as follows: one side of the sample was first polished following the polishing procedure for preparing substrates for deposition. Then two trenches with a gap length of *w* were created. Then one end of the beam was removed, leaving the remaining part of the beam with a length of L. The next step was to remove the steel material below the beam and obtain a beam with height of *b*. Finally, the beam edge was carefully cleaned with low ion beam current again to remove the redeposited materials during the previous FIB milling steps. A diagram of the beam was shown in figure 4.3.1.

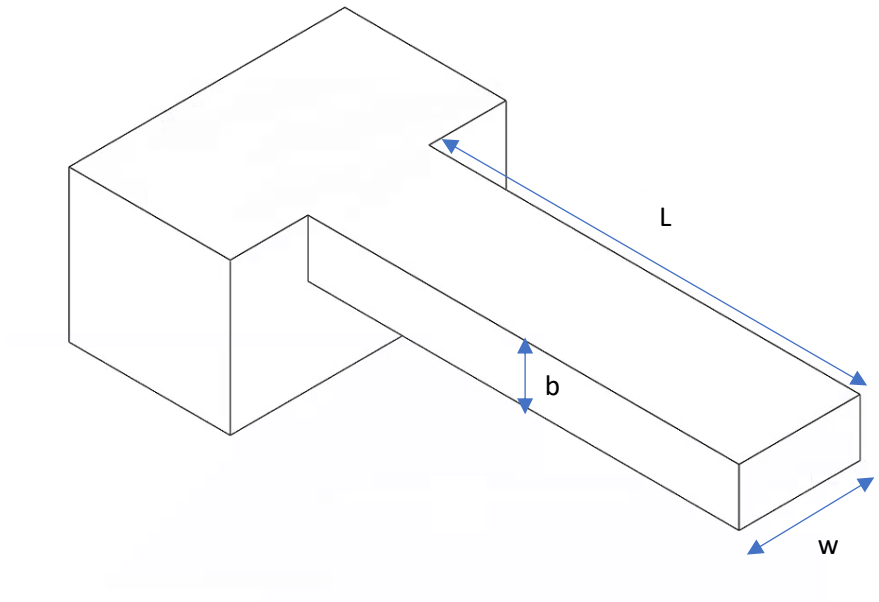


Figure 4.6. A schematic diagram of the microbeam.

Bending test of the microbeam was performed by an in-situ SEM nanoindenter (FT-NMT04, FEMTO). A silicon indenter with a cylinder tip with a flat top, which has a radius about 1um.

The moment of inertia of the beam cross section can be calculated as:

$$I = \frac{wb}{12}(b^2 + w^2) \tag{4.3.1}$$

The mode I fracture toughness $K_{IC}$ can be calculated as:

$$K_{IC} = \sigma_c \sqrt{\pi a} F(\frac{a}{b}) \tag{4.3.2}$$

where $\sigma_c$ is the fracture stress, $a$ is the pre-cracked length of the microbeam. $b$ is the height of the beam and F(a/b) is a dimensionless shaper factor dependent on the beam geometry, which is almost identical to the Srawley and Gross solution, for a/b<0.7 [57]

$$F(\frac{a}{b}) = 1.122 - 1.121(\frac{a}{b}) + 3.74(\frac{a}{b})^2 + 3.873(\frac{a}{b})^3 - 19.05(\frac{a}{b})^4 + 22.55(\frac{a}{b})^5 \tag{4.3.3}$$

For DLC films, the fracture occurs at very small strain. Thus, $\sigma_c$ can be estimated as

$$\sigma = \frac{PLy}{I} \tag{4.3.4}$$

More details about the calculation can be found in these references [57, 58].

## 4.4. Results and discussion

### 4.4.1. Bending test results of microbeam of single Cr/Cr-DLC bilayer DLC film

The microbeam used for the bending test was shown in figure 4.4.1. The notch was cutting be FIB at the 50 pA current, using the line cutting mode. All the beams tested in this experiment was obtained under the same parameters of FIB and hence were supposed to have the same depth. The depth of the notch was gauged to be about 190 nm by cutting a cross section after depositing 1um thick Pt film on it.

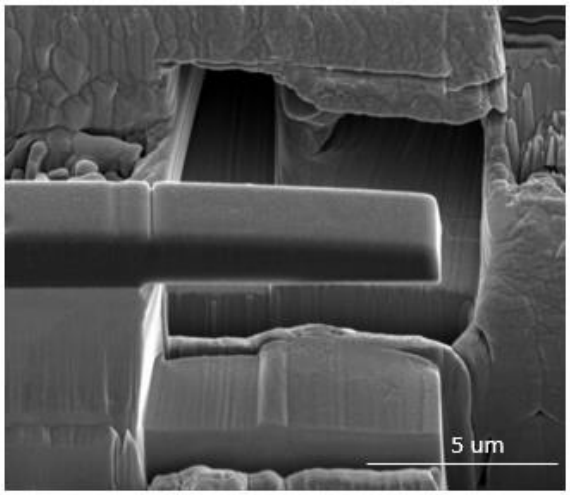


Figure 4.7.A microbeam of DLC130 cut by FIB.

Three beams of sample DLC 130 were cut to do the bending test. Their dimensions and bending test results are shown in table 4.4.1.

Table 4.1. Beam dimensions and calculated fracture toughness of sample DLC130

| Beam | w (um) | l (um) | b (um) | Load(uN) | y(nm) | F(a/b) | $K_{IC}$ (MPa*$m^{1/2}$) |
|---|---|---|---|---|---|---|---|
| Beam 1 | 2.58 | 6.39 | 1.37 | 120.99 | 456 | 1.05 | 0.113 |
| Beam 2 | 2.74 | 7.46 | 1.63 | 107.10 | 597 | 1.05 | 0.102 |
| Beam 3 | 2.04 | 7.41 | 1.59 | 96.43 | 539 | 1.05 | 0.172 |

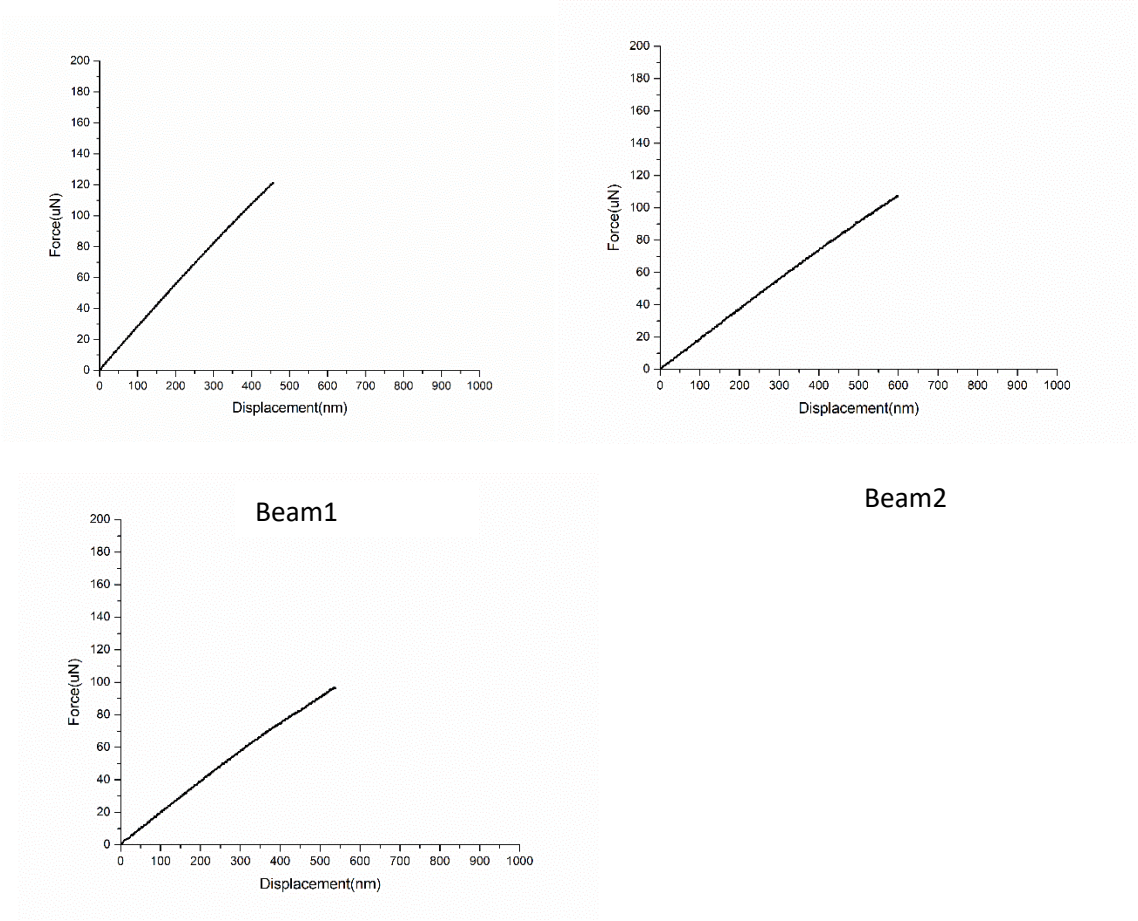


Figure 4.8. Load vs displacement measured during the DLC130 bending test.

4.4.2. Bending test results of microbeam of three Cr/Cr-DLC bilayers of DLC films

The microbeam used for the bending test was shown in figure 4.4.2.

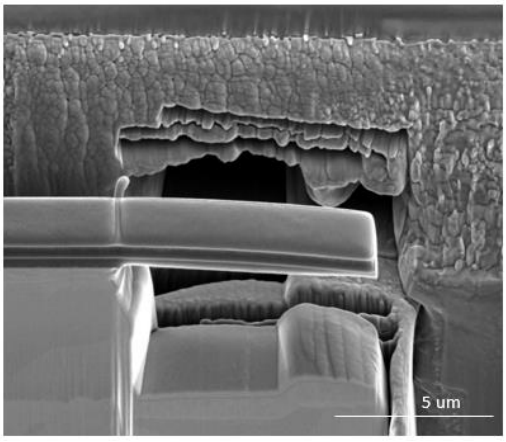


Figure 4.9. Microbeam of DLC134 cut by FIB

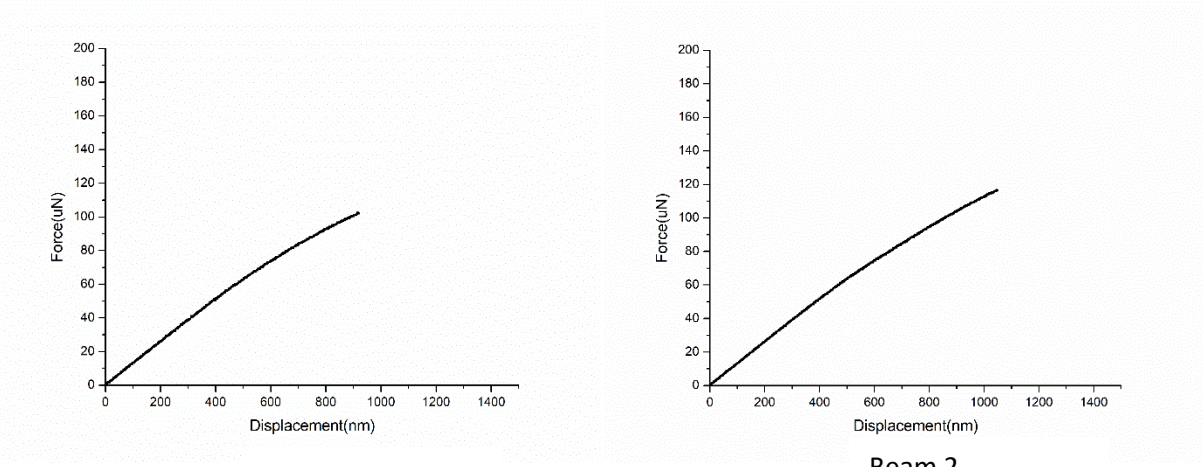


Figure 4.4.4 Load vs displacement curve of DLC134 bending test

Two beams were cut to do the bending test. Their dimensions and bending test results are shown in table 4.4.2

Table 4.2. Beam dimensions and calculated fracture toughness of sample DLC134

| Beam | w (um) | l (um) | b (um) | Load(uN) | y(nm) | F(a/b) | $K_{IC}$ (MPa*$m^{1/2}$) |
|---|---|---|---|---|---|---|---|
| Beam 1 | 2.16 | 7.55 | 0.93 | 116.53 | 1049 | 1.09 | 0.83 |
| Beam 2 | 2.10 | 6.01 | 0.90 | 102.07 | 920 | 1.10 | 0.58 |

The DLC film with three Cr/Cr-DLC bilayers have a five to eight times higher fracture toughness than that of DLC film with a single Cr/Cr-DLC bilayer. It proves that the layer-by-layer method is a useful method to enhance the mechanical properties. This benefit of lay-by-layer multilayer film can come from two aspects: the multilayer DLC films form a complex network structure together with the columnar structure of metallic carbide inside DLC film, with the same mechanism of reinforced concrete structure. This structure will localize the residual stress from accumulation. Also, Cr interlayer will interrupt the growth process of DLC film and introduce tensile stress in the first period of growth stages several times. These tensile residual stress regions will act as a stress relieve region and block the residual stress from accumulation. Moreover, void at the interface between Cr interlayer will also relax the residual stress. Cr interlayer reduces the residual stress in the DLC film. With less residual stress, the DLC film will be harder to fracture. Second, the Cr interlayer can provide a flat base when the DLC film grows thicker, and its surface tends to become rough. Less tiny defects exist on the surface. Third, the crack will be blocked or reduced at the Cr interlayer.

### 4.4.3. Error analysis

This work is an initial exploration on the Cr/Cr-DLC multilayer DLC film and V-notched microbeam bending test on DLC film. From the testing results, it can be judged that the DLC film deposited at this condition is not as brittle as it was supposed to be. As the method is supposed to be used for brittle materials, so some error may come from this deviation. What is more, another error source comes from that the depth of V-notch is set to be a little small to keep the structure of the multilayer in the DLC film. And the depth of the v-notch was gauged independently. These sample are supposed to have a same depth of V-notch with the same FIB parameters. But it might deviate from that value in a degree in practice. This might introduce some errors in calculating the geometry factors and further affects the results of fracture toughness calculation. However, the improvement of fracture toughness of DLC films by several Cr/Cr-DLC bilayers inside the film is obvious under the same measurement conditions in a qualitative way. To get more precise results, further understanding of the properties of DLC films and better control of the bending test of the v-notched microbeam is required.

## Chapter 5. Summary and Conclusion

A new PECVD system has been designed and built to deposit DLC films. Different film growth parameters, like Cr doping, depositing pressure, bias voltage, gas flux, and depositing time, have been investigated to improve the quality of DLC films. The DLC films deposited on silicon wafer at 0.3A Cr target current, 150V bias, the 50:5 ratio of argon and acetylene gas flow flux, 5 mTorr depositing pressure are dense and have a smooth surface. This condition was transferred to deposit DLC films on SS316 substrate after several adjustments were made in the process of plasma etching and Cr interlayer deposition process. Mechanical properties of DLC films deposited at this condition were measured the nanoindentation test. Further these depositing conditions were used to prepare the samples for multilayer DLC films.

Pure Cr interlayer was introduced into the DLC films to make a DLC film consisting of several Cr/Cr-DLC bilayers. A single layer DLC film and a DLC film consisting of three Cr/Cr-DLC bilayers were tested by the bending test of V-notched microbeam. The fracture toughness of the DLC film consisting of three Cr/Cr-DLC bilayers is five to eight times higher than that of the single layer DLC film. It shows that introducing the pure metal interlayer into the DLC film is an effective method to strengthen and toughen the DLC films.

## References


[1] L. B. Freund and S. Suresh, *Thin Film Materials: Stress, Defect Formation and Surface Evolution*, 1st ed. Cambridge University Press, 2004.

[2] Bo Shi, "Intrinsic stress and high temperature properties of metal-containing hydrogenated amorphous carbon coatings. Ph.D. dissertation, Louisana State University.

[3] C. Corbella *et al.*, "Structure of diamond-like carbon films containing transition metals deposited by reactive magnetron sputtering," *Diamond and Related Materials*, vol. 14, no. 3–7, pp. 1103–1107, Mar. 2005.

[4] M. Stueber, H. Holleck, H. Leiste, K. Seemann, S. Ulrich, and C. Ziebert, "Concepts for the design of advanced nanoscale PVD multilayer protective thin films," *Journal of Alloys and Compounds*, vol. 483, no. 1, pp. 321–333, Aug. 2009.

[5] H. Holleck and V. Schier, "Multilayer PVD coatings for wear protection," *Surface and Coatings Technology*, vol. 76–77, pp. 328–336, Nov. 1995.

[6] D. K. Rajak, A. Kumar, A. Behera, and P. L. Menezes, "Diamond-Like Carbon (DLC) Coatings: Classification, Properties, and Applications," *Applied Sciences*, vol. 11, no. 10, p. 4445, May 2021.

[7] C. Donnet and A. Erdemir, Eds., *Tribology of diamond-like carbon films: fundamentals and applications*. New York: Springer, 2008.

[8] K. Bewilogua and D. Hofmann, "History of diamond-like carbon films — From first experiments to worldwide applications," *Surface and Coatings Technology*, vol. 242, pp. 214–225, Mar. 2014.

[9] N. Ohtake *et al.*, "Properties and Classification of Diamond-Like Carbon Films," *Materials*, vol. 14, no. 2, Art. no. 2, Jan. 2021.

[10] K. Jastrzębski, A. Jastrzębska, and D. Bociąga, "A review of mechanical properties of diamond-like carbon coatings with various dopants as candidates for biomedical applications," , *Act Innovations*, No. 22, pp 20-57.

[11] G. Dearnaley and J. H. Arps, "Biomedical applications of diamond-like carbon (DLC) coatings: A review," *Surface and Coatings Technology*, vol. 200, no. 7, pp. 2518–2524, Dec. 2005.

[12] A. Grill, “Electrical and optical properties of diamond-like carbon,” *Thin Solid Films*, vol. 355–356, pp. 189–193, Nov. 1999.

[13] H. Moriguchi, H. Ohara, and M. Tsujioka, “History and Applications of Diamond-Like Carbon Manufacturing Processes,” *SEI Technical Review*, Number 82, April 2016.

[14] J. Vetter, “60 years of DLC coatings: Historical highlights and technical review of cathodic arc processes to synthesize various DLC types, and their evolution for industrial applications,” *Surface and Coatings Technology*, vol. 257, pp. 213–240, Oct. 2014.

[15] D. S. Mao *et al.*, “Electron field emission from a patterned diamond-like carbon flat thin film using a Ti interfacial layer,” *J. Vac. Sci. Technol. B*, vol. 18, no. 5, p. 2420, 2000.

[16] Meškinis, Vasiliauskas, Viskontas, Andrulevičius, Guobienė, and Tamulevičius, “Hydrogen-Free Diamond Like Carbon Films with Embedded Cu Nanoparticles: Structure, Composition and Reverse Saturable Absorption Effect,” *Materials*, vol. 13, no. 3, p. 760, Feb. 2020.

[17] T. F. Zhang, Z. X. Wan, J. C. Ding, S. Zhang, Q. M. Wang, and K. H. Kim, “Microstructure and high-temperature tribological properties of Si-doped hydrogenated diamond-like carbon films,” *Applied Surface Science*, vol. 435, pp. 963–973, Mar. 2018.

[18] G. Gassner, P. H. Mayrhofer, C. Mitterer, and J. Kiefer, “Structure–property relations in Cr–C/a-C:H coatings deposited by reactive magnetron sputtering,” *Surface and Coatings Technology*, vol. 200, no. 1–4, pp. 1147–1150, Oct. 2005.

[19] I. Bouabibsa, S. Lamri, and F. Sanchette, “Structure, Mechanical and Tribological Properties of Me-Doped Diamond-Like Carbon (DLC) (Me = Al, Ti, or Nb) Hydrogenated Amorphous Carbon Coatings,” *Coatings*, vol. 8, no. 10, p. 370, Oct. 2018.

[20] J. C. Jiang, W. J. Meng, A. G. Evans, and C. V. Cooper, “Structure and mechanics of W-DLC coated spur gears,” *Surface and Coatings Technology*, vol. 176, no. 1, pp. 50–56, Nov. 2003.

[21] C. Donnet, “Recent progress on the tribology of doped diamond-like and carbon alloy coatings: a review,” *Surface and Coatings Technology*, vol. 100–101, pp. 180–186, Mar. 1998.

[22] A. Banerji, S. Bhowmick, and A. T. Alpas, “High temperature tribological behavior of W containing diamond-like carbon (DLC) coating against titanium alloys,” *Surface and Coatings Technology*, vol. 241, pp. 93–104, Feb. 2014.

[23] W. J. Meng and B. A. Gillispie, “Mechanical properties of Ti-containing and W-containing diamond-like carbon coatings,” *Journal of Applied Physics*, vol. 84, no. 8, pp. 4314–4321, Oct. 1998.

[24] Meng-Yuan Tsai, et al., “Surface properties of copper-incorporated diamond-like carbon films deposited by hybrid magnetron sputtering", Ceramics International, vol. 39, Sep. 2013

[25] F. P. Schwarz, I. Hauser-Gerspach, T. Waltimo, and B. Stritzker, “Antibacterial properties of silver containing diamond like carbon coatings produced by ion induced polymer densification,” *Surface and Coatings Technology*, vol. 205, no. 20, pp. 4850–4854, 2011.

[26] R. Paul, “Diamond-Like-Carbon Coatings for Advanced Biomedical Applications,” p. 5.

[27] S. Aisenberg and F. M. Kimock, “Ion Beam and Ion-Assisted Deposition of Diamond-Like Carbon Films,” *MSF*, vol. 52–53, pp. 1–40, Jan. 1991.

[28] A. C. Ferrari *et al.*, “Density, sp^3 fraction, and cross-sectional structure of amorphous carbon films determined by x-ray reflectivity and electron energy-loss spectroscopy,” *Phys. Rev. B*, vol. 62, no. 16, pp. 11089–11103, Oct. 2000

[29] Y. Liu, A. Erdemir, and E. I. Meletis, “A study of the wear mechanism of diamond-like carbon films,” *Surface and Coatings Technology*, vol. 82, no. 1, pp. 48–56, Jul. 1996

[30] H. Hofsäss, H. Binder, T. Klumpp, and E. Recknagel, “Doping and growth of diamond-like carbon films by ion beam deposition,” *Diamond and Related Materials*, vol. 3, no. 1, pp. 137–142, Jan. 1994

[31] Shi Xu et al., “Properties of carbon ion deposited tetrahedral amorphous carbon films as a function of ion energy", Journal of Applied Physics: Vol 79, No 9.

[32] A. A. Voevodin and M. S. Donley, “Preparation of amorphous diamond-like carbon by pulsed laser deposition: a critical review,” *Surface and Coatings Technology*, vol. 82, no. 3, pp. 199–213, Aug. 1996.

[33] G. Fedosenko, A. Schwabedissen, J. Engemann, E. Braca, L. Valentini, and J. M. Kenny, “Pulsed PECVD deposition of diamond-like carbon films,” *Diamond and Related Materials*, vol. 11, no. 3–6, pp. 1047–1052, Mar. 2002.

[34] J. Robertson, “Comparison of diamond-like carbon to diamond for applications,” *phys. stat. sol. (a)*, vol. 205, no. 9, pp. 2233–2244, Sep. 2008.

[35] J. K. Luo, Y. Q. Fu, H. R. Le, J. A. Williams, S. M. Spearing, and W. I. Milne, "Diamond and diamond-like carbon MEMS," *J. Micromech. Microeng.*, vol. 17, no. 7, pp. S147–S163, Jul. 2007.

[36] A. Grill, "Tribology of diamondlike carbon and related materials: an updated review," *Surface and Coatings Technology*, vol. 94–95, pp. 507–513, Oct. 1997.

[37] J. A. Williams and H. R. Le, "Tribology and MEMS," *J. Phys. D: Appl. Phys.*, vol. 39, no. 12, pp. R201–R214, Jun. 2006.

[38] D. M. Cao, T. Wang, B. Feng, W. J. Meng, and K. W. Kelly, "Amorphous hydrocarbon based thin films for high-aspect-ratio MEMS applications," *Thin Solid Films*, vol. 398–399, pp. 553–559, Nov. 2001.

[39] D. Kim, D. Cao, M. D. Bryant, W. Meng, and F. F. Ling, "Tribological Study of Microbearings for MEMS Applications," *Journal of Tribology*, vol. 127, no. 3, pp. 537–547, Jan. 2005.

[40] R. Jethanandani, "The development and application of diamond-like carbon films," *JOM*, vol. 49, no. 2, pp. 63–65, Feb. 1997.

[41] R. Hang, M. Zhang, S. Ma, and P. K. Chu, "Biological response of endothelial cells to diamond-like carbon-coated NiTi alloy," *J Biomed Mater Res A*, vol. 100, no. 2, pp. 496–506, Feb. 2012.

[42] R. K. Roy and K.-R. Lee, "Biomedical applications of diamond-like carbon coatings: a review," *J Biomed Mater Res B Appl Biomater*, vol. 83, no. 1, pp. 72–84, Oct. 2007.

[43] R. Hauert, K. Thorwarth, and G. Thorwarth, "An overview on diamond-like carbon coatings in medical applications," *Surface and Coatings Technology*, vol. 233, pp. 119–130, Oct. 2013.

[44] R. Lappalainen and S. S. Santavirta, "Potential of Coatings in Total Hip Replacement.," *Clinical Orthopaedics and Related Research (1976-2007)*, vol. 430, pp. 72–79, Jan. 2005.

[45] L. Chandra, M. Allen, R. Butter, N. Rushton, A. H. Lettington, and T. W. Clyne, "The effect of exposure to biological fluids on the spallation resistance of diamond-like carbon coatings on metallic substrates," *J Mater Sci: Mater Med*, vol. 6, no. 10, pp. 581–589, Oct. 1995.

[46] A. H. Lettington, “Applications of diamond-like carbon thin films,” in *Thin Film Diamond*, A. H. Lettington and J. W. Steeds, Eds. Dordrecht: Springer Netherlands, 1994, pp. 117–126.

[47] Mary F. Doerner and William D. Nix, “Stresses and deformation processes in thin films on substrates", Critical Reviews in Solid State and Materials Sciences: Vol 14, No 3. pp. 225-268.

[48] L. Liu *et al.*, “Excellent adhered thick diamond-like carbon coatings by optimizing hetero-interfaces with sequential highly energetic Cr and C ion treatment,” *Journal of Alloys and Compounds*, vol. 735, pp. 155–162, Feb. 2018.

[49] M. S. Kabir, Z. Zhou, Z. Xie, and P. Munroe, “Designing multilayer diamond like carbon coatings for improved mechanical properties,” *Journal of Materials Science & Technology*, vol. 65, pp. 108–117, Feb. 2021.

[50] Z. Xu, Y. J. Zheng, F. Jiang, Y. X. Leng, H. Sun, and N. Huang, “The microstructure and mechanical properties of multilayer diamond-like carbon films with different modulation ratios,” *Applied Surface Science*, vol. 264, pp. 207–212, Jan. 2013.

[51] M. Cui, J. Pu, J. Liang, L. Wang, G. Zhang, and Q. Xue, “Corrosion and tribocorrosion performance of multilayer diamond-like carbon film in NaCl solution,” *RSC Adv.*, vol. 5, no. 127, pp. 104829–104840, Dec. 2015.

[52] C. Strondl *et al.*, “Properties and characterization of multilayers of carbides and diamond-like carbon,” *Surface and Coatings Technology*, vol. 142–144, pp. 707–713, Jul. 2001.

[53] M. Cui, J. Pu, G. Zhang, L. Wang, and Q. Xue, “The corrosion behaviors of multilayer diamond-like carbon coatings: influence of deposition periods and corrosive medium,” *RSC Adv.*, vol. 6, no. 34, pp. 28570–28578, Mar. 2016.

[54] W. Zhang, A. Tanaka, B. S. Xu, and Y. Koga, “Study on the diamond-like carbon multilayer films for tribological application,” *Diamond and Related Materials*, vol. 14, no. 8, pp. 1361–1367, Aug. 2005.

[55] C. Rincón *et al.*, “Tungsten carbide/diamond-like carbon multilayer coatings on steel for tribological applications,” *Surface and Coatings Technology*, vol. 148, no. 2, pp. 277–283, Dec. 2001.

[56] N. Dwivedi, S. Kumar, and H. K. Malik, “Nanostructured Titanium/Diamond-Like Carbon Multilayer Films: Deposition, Characterization, and Applications,” *ACS Appl. Mater. Interfaces*, vol. 3, no. 11, pp. 4268–4278, Nov. 2011.

[57] X. Zhao, R. M. Langford, J. Tan, and P. Xiao, “Mechanical properties of SiC coatings on spherical particles measured using the micro-beam method,” *Scripta Materialia*, vol. 59, no. 1, pp. 39–42, Jul. 2008.

[58] D. Di Maio and S. G. Roberts, “Measuring fracture toughness of coatings using focused-ion-beam-machined microbeams,” *J. Mater. Res.*, vol. 20, no. 2, pp. 299–302, Feb. 2005.

[59] M. Zhong, C. Zhang and J. Luo, "Effect of substrate morphology on the roughness evolution of ultra-thin DLC films," *Applied Surface Science*, vol. 254, pp. 6742-6748, Apr. 2008.

# Vita

Tailei Qi received his bachelor's (2015) degree from the Department of Physics of Wuhan University in China. He worked at Suzhou Advanced Materials Research Institute and South University of Science and Technology before he became a graduate student in the Mechanical and Industrial Engineering Department at Louisiana State University in August 2019. He plans to receive his Master's degree in material science and engineering in December 2021, and he is well prepared for the new challenges.